HHS Public Access

Author manuscript

Cell Rep. Author manuscript; available in PMC 2024 January 29.

Published in final edited form as:

Cell Rep. 2023 October 31; 42(10): 113128. doi:10.1016/j.celrep.2023.113128.

Pannexin-1 opening in neuronal edema causes initial cell death but also leads to protection via increased microglia contacts

Nicholas L. Weilinger[*,1], **Kai Yang**[*,1], **Hyun B. Choi**[*,1], **Christopher J. Groten**[1], **Stefan Wendt**[1], **Madhuvika Murugan**[3], **Leigh E. Wicki-Stordeur**[1], **Louis-Philippe Bernier**[1], **Prashanth S. Velayudhan**[1], **Jiaying Zheng**[3], **Jeffrey M. LeDue**[1], **Ravi L. Rungta**[1], **John R. Tyson**[1,2], **Terrance P. Snutch**[1,2], **Long-Jun Wu**[3], **Brian A. MacVicar**[1]

[1.]Djavad Mowafaghian Centre for Brain Health, University of British Columbia, Vancouver, V6T 1Z3, Canada

[2.]Michael Smith Laboratories, University of British Columbia, Vancouver, V6T 1Z4, Canada

[3.]Department of Neurology, Mayo Clinic, Rochester, MN 55905, USA

Abstract

Neuronal swelling during cytotoxic edema is triggered by Na^+ and Cl^- entry and is Ca^{2+}-independent. However, the causes of subsequent neuronal death after swelling are a longstanding puzzle. We tested if the large-conductance Pannexin-1 (Panx1) channel contributes to cytotoxic death. Panx1 channel inhibitors reduced and delayed neuronal death when swelling was triggered by intense voltage-gated Na^+ entry and subsequent Cl^- entry. We show that neuronal swelling triggered oxidative stress via reactive oxygen species (ROS) that in turn caused cytotoxic Panx1 opening. ROS activated Panx1 currents in whole-cell recordings and ROS scavengers inhibited Panx1 currents and were neuroprotective in swelling assays. Panx1 opening and subsequent ATP release recruited microglial processes to contact swelling neurons. Depleting microglia using the CSF1 receptor antagonist PLX3397 or blocking P2Y12 receptors exacerbated cytotoxic death of neurons suggesting that the Panx1- and ATP-dependent enhancement of surveillance by microglia is neuroprotective. We conclude that cytotoxic edema triggers oxidative stress in neurons that in turn opens Panx1 to trigger neuronal death, but also initiates neuroprotective feedback mediated by microglia contacts.

Correspondence to: bmacvicar@brain.ubc.ca.

*Co-first authors

Author contributions:

N.L.W. performed PI-loading and microglia contact experiments and wrote the manuscript with B.A.M.. K.Y. performed and analyzed acutely isolated patch clamp experiments. H.B.C. performed and analyzed LDH release, lipid peroxidation, and ascorbic acid measurement experiments. C.J.G. performed and analyzed single cell osmotic swelling patch clamp experiments as well as microglia contact experiments. M.M. conducted microglia contact experiments in $P2Y_{12}R^{-/-}$ mice in the lab of L.J.W. L.E.W.S. performed all western-blot experiments. H.B.C., J.R.T., J.L., T.P.S. and B.A.M. developed the slice swelling assay. P.S.V. performed slice swelling experiments with H.B.C.. J.L. developed the image analysis software pipeline. R.L.R., J.R.T. and L.P.B. performed preliminary experiments. All authors reviewed and edited the manuscript. L.J.W. and B.A.M. designed and supervised the study.

Competing interests: Authors declare no competing interest.

Introduction

Brain swelling, or edema, is a major cause of mortality after stroke, traumatic brain injury (TBI), and other insults (Donkin and Vink, 2010; Simard et al., 2007). Cytotoxic swelling of nerve cells stems from perturbations in ionic gradients that occur during excitotoxicity such as in ischemic depolarization (Dreier et al., 2018; Liang et al., 2007; Weilinger et al., 2016; Zhou et al., 2010), resulting in an increase in tonicity and osmotic pressure of the cytosolic compartment (Choi, 1987; Dreier et al., 2018; Hasbani et al., 1998; Rothman, 1985; Rungta et al., 2015). We reported a key role for the Cl^- channel SLC26A11 that is principally responsible for Cl^- dysregulation and swelling in cytotoxic edema, leading to death over minutes to hours (Rungta et al., 2015). This neuronal death in cytotoxic edema is Ca^{2+}-independent (Rothman, 1985; Rungta et al., 2015) and therefore distinct from canonical pathways described in ischemia (Lipton, 1999), but the mechanistic links between neuronal swelling and death are otherwise unresolved.

We explored potential roles for the large-pore ion and metabolite channel Pannexin-1 (Panx1)(Bialecki et al., 2019; Boyce et al., 2018; Chiu et al., 2018) in cytotoxic death in light of its role in necrosis (Thompson et al., 2006; Weilinger et al., 2013) and apoptosis as a conduit for ATP release to recruit the inflammasome (Chekeni et al., 2010; Sandilos et al., 2012). Panx1 activation is multimodal (Chiu et al., 2018), with early work in erythrocytes and epithelial cells suggesting it could operate as a mechanosensitive channel, making it a likely candidate in cytotoxic swelling. This view was more recently challenged, however, with the discovery that mechanical Panx1 opening occurred downstream of *bona fide* mechanosensitive Piezo1 channels (Cahalan et al., 2015; Cinar et al., 2015; Ranade et al., 2014). Previous work by us and others have shown that Panx1 harbors multiple sites for posttranslational modifications (Chekeni et al., 2010; Chiu et al., 2018; Lohman et al., 2019; Thompson et al., 2008; Weilinger et al., 2016; Weilinger et al., 2012), and channel opening is sensitive to oxidation-reduction (redox) states (Bunse et al., 2011; Bunse et al., 2010; Lohman et al., 2012b; Prochnow et al., 2009; Wang and Dahl, 2010; Xu et al., 2018; Zhang et al., 2008). Interestingly, swelling-induced generation of reactive oxygen species (ROS) can occur due to neuronal membrane stretch (Arundine et al., 2004; Brandes et al., 2014; Ji et al., 2012; Shah et al., 1997), hinting at possible links to Panx1 opening.

The implications for ATP release due to Panx1 opening (Chekeni et al., 2010; Sandilos et al., 2012) are not limited to the induction of neurotoxicity. Microglia, the innate immune cells of the brain, are highly dynamic and extend their processes towards damage in an ATP-dependent manner that is neuroprotective in models of epilepsy and stroke (Badimon et al., 2020; Cserép et al., 2020; Eyo et al., 2014; Kato et al., 2016; Szalay et al., 2016; Wake et al., 2009). This chemoattractive ‘find-me’ process is transduced by the G protein-coupled purinergic receptor $P2Y_{12}R$ expressed exclusively in microglia (Haynes et al., 2006; Honda et al., 2001; Sasaki et al., 2003), however mechanisms for upstream ATP release are yet to be resolved (Dissing-Olesen et al., 2014; Eyo et al., 2014; Eyo and Wu, 2019; Li et al., 2012). Here we test our hypothesis for a dichotomous role of Panx1 channel opening in edema: (i) that cytotoxic death in swelling is precipitated by Panx1 opening; and (ii) that concurrent Panx1-ATP release during this death process triggers a neuroprotective response from microglia. We show that neuronal swelling directly leads to cell death that is sensitive

to pharmacological or genetic disruption of Panx1 and ROS scavenging. We provide direct evidence that cellular oxidation occurs during neuronal swelling using a ratiometric redox sensor, roGFP1, and that exogenously supplied ROS activates Panx1 currents in rat and mouse cortical neurons. Finally, we show that Panx1 opening in edema attracts microglia extensions (Eyo et al., 2015; Eyo et al., 2014), a process that we confirm is neuroprotective using selective microglia depletion with PLX3397 (Elmore et al., 2014). The identification of a ROS-Panx1 activation in cytotoxic edema is a critical step to understanding neuronal death, but also highlights important complications associated with therapeutic targeting of Panx1 to prevent cell death given its neuroprotective role via ATP release.

Results

Cell death in edema is attenuated with Panx1 channel inhibitors and genetic knockdown

Neuronal swelling can be initiated by Na^+ influx through voltage-gated Na^+ channels and/or ionotropic glutamate receptors (Hasbani et al., 1998; Rothman, 1985; Rungta et al., 2015). As a first step, we induced cytotoxic edema in acute rat cortical and hippocampal brain slice preparations using veratridine (50 μM) to trigger Na^+-channel opening and subsequent Cl^- loading as we have described previously (Fig. 1a–f)(Rungta et al., 2015). To isolate swelling induced cell death from glutamate excitotoxicity and Ca^{2+}-dependent necrosis, we co-applied inhibitors of glutamatergic NMDA (D-APV, 50 μM) and AMPA (CNQX, 10 μM) receptors, as well as voltage-gated calcium channels ($CdCl_2$, 50 μM) and GABA activated Cl^- channel (picrotoxin, PTX, 100 μM) blockers (Rungta et al., 2015). Veratridine administered either by local ejection with a puff electrode (Fig. 1a–c) or by bath application (Fig. 1d–f) caused a rapid volume increase in individual neurons and whole brain slices as measured by changes in cross-sectional area. Veratridine-induced cytotoxic swelling was dramatically attenuated when the extracellular Cl^- concentration was reduced from 136 mM (control) to 20 mM (low$[Cl^-]_o$), confirming the requirement of Cl^- influx (Rothman, 1985; Rungta et al., 2015; Weilinger et al., 2022).

We next examined the potential role of Panx1 opening in swelling-induced necrosis by applying Panx1 channel inhibitors (Fig. 1g) or performing experiments in $Panx1^{-/-}$ transgenic mice (Fig. 1h,i)(Penuela et al., 2009). In acute cortical brain slices from rats, transient (15 min) bath application of veratridine caused neuronal edema and cell death quantified by lactate dehydrogenase (LDH) release 90 min post-insult as a measure of membrane permeabilization (Fig. 1g). This LDH release was inhibited by the Panx1 blockers ^{10}panx (Thompson et al., 2008) or probenecid (Silverman et al., 2008) while the scrambled control for ^{10}panx (^{SC}panx) had no effect (Fig. 1g). LDH release was similarly reduced in brain slices from $Panx1^{-/-}$ transgenic mice (Qu et al., 2011) compared to wild-type controls ($Panx1^{WT}$, Fig. 1h). Interestingly, there was no effect of knocking out Panx1 on the rate or severity of veratridine-evoked whole tissue swelling (Fig. S1a,b), suggesting that Panx1 opening occurs downstream of water entry and a volume increase.

The temporal progression of Panx1-dependent cell death was also examined by quantifying cellular staining by propidium iodide (PI, 668 Da, 20 μM), a well-characterized neuronal death marker that enters cells during membrane damage (Lau et al., 2007; Wilde et al., 1994) but should also permeate the Panx1 channel pore (~0.9kDa). PI staining was quantified in

brain slices by SNAPSHOT flash-fixation (Dissing-Olesen and MacVicar, 2015) at several time points after a veratridine insult (Fig. 1j). Two-photon microscopy analysis of PI loading in control conditions revealed few PI positive cells within the normally healthy slice center (Fig. 1k) and an expected pattern of fluorescence close (<70 μm) to the slice surface due to damage from preparing brain slices (Bak et al., 1980; Dzhala et al., 2012). In contrast, transient veratridine exposure (15 min) triggered progressive PI staining of neurons in the initially healthy slice interior that was not observed in untreated controls (Fig. 1k). PI staining density was attenuated by the Panx1 inhibitors carbenoxolone (CBX) (Fig. 1k–m, (Thompson et al., 2006)) and ^{10}panx, confirming that Panx1 opening contributes to swelling-induced death (Fig. 1n). To test whether this Panx1 opening triggered apoptotic death (Chekeni et al., 2010), we probed for activated caspase-3 (casp3), a core effector protease and marker of apoptosis (Eldadah and Faden, 2000), and found no increase after veratridine exposure (Fig S2). Similarly, we did not detect Panx1 cleavage products that would be expected in apoptosis (Fig S3)(Chekeni et al., 2010; Sandilos et al., 2012). Together, these data indicate Panx1 activation in edema likely triggers necrotic death similar to ischemia (Weilinger et al., 2016).

Next, we sought to confirm that osmotic swelling itself activated Panx1 independent of veratridine. Pyramidal neurons were whole-cell patch clamped with a high osmolarity internal solution (30% increase to 380 mOsm) and Alexa 350 (100 μM) to drive osmotic water entry and visualize swelling, respectively. In this way, we could reliably induce swelling that was restricted to the patched cell, allowing for reliable image analysis. Extracellular artificial cerebrospinal fluid (ACSF) contained PI (40 μM) to monitor cell death. In high osmolarity recordings, neuronal cross-sectional area increased immediately and continuously after whole-cell access was attained compared to 290 mOsm controls (Fig. S4a–e). Progressive swelling culminated in membrane breakdown and lysis, as evidenced by PI accumulation and increased holding current (Fig. S4a–f). Neurons pretreated with either ^{10}panx or ^{SC}panx exhibited similar swelling and characteristic swelling-associated currents, likely mediated by volume regulated anion channels (VRACs) such as LRRC8 (Fig. S4g–k)(Okada et al., 2019). However, PI staining in ^{10}panx treated neurons was significantly delayed compared to ^{SC}panx controls, suggesting a greater tolerance to swelling stress when Panx1 channels are blocked (Fig. S4l,m). Collectively, these data point to Panx1-dependent neuronal death that is delayed minutes from the swelling onset, consistent with the timing of protection afforded by ^{10}panx and CBX in the PI loading and LDH release experiments (Fig. 1).

Cytotoxic edema triggers oxidative stress in neurons

Oxidative stress is associated with a host of neuronal pathologies (Angelova and Abramov, 2018) including membrane stretch (Arundine et al., 2004; Brandes et al., 2014), and Panx1 channel opening is sensitive to redox changes (Bunse et al., 2009; Bunse et al., 2011; Bunse et al., 2010; Lohman et al., 2012b; Onami et al., 2014; Wang and Dahl, 2010). We therefore postulated that Panx1 activation in edema was triggered by ROS generated during neuronal swelling. To assess the spatiotemporal progression of neuronal redox states during swelling, we used roGFP1, a genetically encoded fluorescent protein that provides ratiometric readouts of cytoplasmic redox states. Neuronal roGFP1 expression was induced

via AAV delivery in rat pups that were later used for time series recordings in acute brain slices 2–3 weeks post-injection. Importantly, as described in our recent publication (Wendt et al., 2022), the ratiometric properties of roGFP1 allow for comparisons of relative cytoplasmic oxidative stress even during volume changes. The redox changes in neurons can be detected when green fluorescence emission (~500–550 nm) from excitation at 740 nm (peak emission when oxidized) and 910 nm (peak emission when reduced) are quantified and ratioed (Wendt et al., 2022)(Fig. 2a). Alternating excitation wavelengths allows for continuous time series recordings of neuronal redox states. As a first step, we tested the functional readouts of the emission ratios by exposing neurons expressing roGFP1 to hydrogen peroxide (H_2O_2). At rest, roGFP1 ratios in neurons were consistent with a more reduced redox state (Fig. 2a,b). Transient H_2O_2 application by puff electrode (8 mM, 5 min) triggered rapid oxidation in neurons, with roGFP1 ratios increasing ~1.5 fold over baseline (Fig. 2a,b).

To test whether swelling increased cytoplasmic ROS, veratridine was locally applied by pressure ejection from an adjacent electrode to minimize the extent of whole-tissue swelling, permitting stable roGFP1 readouts in neurons (Fig. 2c). Neuronal swelling triggered cytosolic oxidation in cortical neurons which peaked within minutes of the stimulus onset (Fig. 2c–f). This oxidative shift occurred in tandem with somatic swelling (Fig. 2g), indicating that swelling and oxidation temporally coincided. Using the criteria that cells were responders if the change in 740/910 nm excitation ratio was >2 standard deviations from baseline variation (Fig. 2h), we found that 72.4% of neurons in the imaging plane were oxidized as neuronal edema developed. As an important control, preventing veratridine-evoked swelling with low $[Cl^-]_o$ ACSF and DIDS (1 mM), a non-selective Cl^- channel blocker (Rungta et al., 2015), significantly reduced the proportion of oxidized cells to 23.9% (Fig. 2i), confirming that this oxidation is swelling-dependent and that veratridine application or Na^+ entry are not sufficient. Thus, these data affirm that swelling itself is sufficient to trigger cytosolic oxidation in a large fraction of cortical neurons.

Swelling-induced death requires ROS accumulation

To further investigate the correlation of neuronal swelling with ROS generation we measured swelling-induced lipid peroxidation, a hallmark of oxidative stress, in whole-brain slices (Zhang et al., 2014). Bath application of veratridine in the presence of glutamatergic and GABAergic blockers (APV, CNQX, PTX) increased lipid peroxidation in slices relative to naive tissue (Fig. 3a). Applying xanthine/xanthine oxidase (X/XO, [X]= 20 μg/mL and [XO]= 25 μg/mL)(Zhang et al., 2014) to directly generate superoxide (O_2^-) and H_2O_2 (Fig. 3a) also induced lipid peroxidation in treated slices. This increase in lipid peroxidation by oxidizing agents or by neuronal swelling was not reduced in $Panx1^{-/-}$ animals nor by blocking Panx1 channels with probenecid (Fig. 3b,c), indicating that swelling-induced ROS generation is not Panx1-dependent. As a control, lipid peroxidation in veratridine was attenuated when neuronal swelling was reduced with low$[Cl^-]_o$ (Fig. 3c), corroborating results that Na^+ loading and/or depolarization alone are not sufficient to trigger ROS generation.

Ascorbic acid (AA) is the principal endogenous antioxidant in neurons (10 mM) with intracellular concentrations ~10-fold higher than in astrocytes (Rice, 2000). AA is protective in models of neurodegeneration by buffering oxidative stress (Rice, 2000), so we tested whether AA concentrations were altered in veratridine as a measure of neuronal oxidative stress. Exposure of brain slices to veratridine progressively reduced AA levels (measured from whole tissue homogenate) compared to controls (Fig. 3d) suggesting that ROS-dependent cell death could be a consequence not only of increased ROS formation but also that decreased ROS scavenging could contribute. We directly tested the neuroprotective efficacy of ROS scavengers N-acetyl cysteine (NAC, 5 mM) or trolox (100 μM) in veratridine and measured reductions in LDH release and PI uptake (Fig. 3e,f), whereas tissue swelling was unaffected (Fig. S5). Together, these data point to a sequelae initiated by swelling that leads to ROS accumulation and subsequent Panx1-dependent neuronal death.

ROS activates Panx1 channel currents

If Panx1 channels are opened by oxidative stress, then exogenously applied ROS should generate Panx1 currents in the absence of swelling. We tested this by bath applying X/XO or H_2O_2 during whole cell voltage clamp recordings of acutely isolated pyramidal neurons from the hippocampus. This strategy was used to overcome space clamp issues, provided fast/reliable pharmacological access, and circumvented endogenous ROS scavenging by glia (Bolaños, 2016) in acute brain slices. In patched neurons from $Panx1^{WT}$ mice, X/XO induced a typical non-selective current characteristic of Panx1 channel opening (Thompson et al., 2006) that was absent in $Panx1^{-/-}$ neurons (Fig. 4a,b,h). Similar Panx1 currents were observed using H_2O_2 (Fig. S6). These data were confirmed in rat neurons, where X/XO activated a Panx1 current that was blocked by pre-application of CBX or probenecid, ^{10}panx, or an intracellularly dialyzed c-terminal antibody (ab-panx (Weilinger et al., 2012)) (Fig. 6c,d,g). X/XO-Panx1 currents were not blocked by inhibitors of other ROS-sensitive channels, such as TRPV1/2 and TRPM2 channels, nor by the pan-caspase inhibitor ZVAD (Fig. S7).

Recordings from the preceding electrophysiology experiments on acutely isolated pyramidal neurons were performed in the absence of AA and therefore endogenous AA was diluted when whole-cell patch mode was attained. We tested the hypothesis that enhancing intracellular ROS scavenging could prevent Panx1 activation in X/XO. Indeed, X/XO activated Panx1 currents were inhibited by including AA in the pipette (AA_i 10mM, (Rice, 2000)), as well as by bath application of NAC, whereas the negative control xanthine alone failed to open Panx1 (Fig. 4e,f). These data collectively show that Panx1 can be opened by ROS that is sensitive to antioxidants.

ROS-Panx1 opening in swelling increases microglia-neuron contacts

Microglia are the resident immune cells of the brain that respond to damage via ATP-dependent chemotaxis and process extension (Davalos et al., 2005). We hypothesized that Panx1 opening in edema would attract microglia to swelling neurons similar to models of epilepsy and ischemia (Cserép et al., 2020; Eyo et al., 2014; Kato et al., 2016; Szalay et al., 2016; Wake et al., 2009). As a first confirmation, we tested for ATP release in a hypotonic perfusate model of swelling and found a significant increase in extracellular

ATP levels that was absent in Panx1$^{-/-}$ mice (Fig S8). If cytotoxic ATP release through Panx1 is sufficient to mobilize microglia processes, then an increase in microglia contacts should be observed during neuronal swelling that is sensitive to Panx1 block. To control for potential confounds from autocrine microglia ATP release in hypotonic perfusate models of swelling (Murana et al., 2017), we used a single-cell approach to restrict cytotoxic edema to individual whole-cell patched neurons (similar to Fig. S4) in CX3CR1$^{EGFP/+}$ mice to simultaneously monitor microglia surveillance in surrounding tissue. Neurons were patch-loaded with a hyperosmotic recording solution (380 mOsm) containing Alexa 594 to visualize cell swelling and coincident EGFP-positive microglia contacts were compared to an iso-osmotic control (Fig. 5a,b). We consistently observed pre-existing microglia contacts on neuronal somata (Fig 5a–d), measured immediately following whole-cell breakthrough, and found no difference in baseline contacts between hypertonic and isotonic conditions (Fig 5e). Intracellular dialysis of hypertonic recording solution triggered progressive neuronal swelling and a stark increase in microglia contacts compared to isotonic controls (Fig 5a–d,f). Although recording times were reduced because of cell loss in hypertonic stress conditions (Fig S4f, Fig 5g,h), we observed an increase in microglia-neuron contact rates in swelling compared to controls (Fig 5g,i).

Next, we tested whether microglia-neuron contacts were guided by Panx1-dependent ATP release (Chekeni et al., 2010; Sandilos et al., 2012). Bath application of the mimetic peptide inhibitor ^{10}panx significantly reduced the microglia contact frequency in hypertonic swelling compared to the scrambled peptide ^{SC}panx (Fig. 5j). As an important control, we found no effect of ^{10}panx on basal microglia surveillance, nor on microglia convergences in a laser burn lesion model (Davalos et al., 2005; Hines et al., 2009)(Fig. S9), together indicating that Panx1 block is specific to neuronal ATP release in swelling. Finally, the role for P2Y$_{12}$R in microglia process extensions was validated in P2Y$_{12}$R$^{-/-}$ mice, where we observed a marked reduction in microglia process convergences in swelling (Fig. S10)(Eyo et al., 2015; Eyo et al., 2014), confirming that microglia P2Y$_{12}$R is vital for ATP chemotaxis (Davalos et al., 2005; Haynes et al., 2006). Together these data indicate that Panx1 is the conduit for ATP release in cytotoxic swelling that guides microglia processes via P2Y$_{12}$R signaling.

Panx1-microglia signaling is neuroprotective in edema

Emerging evidence suggests that microglial contacts on neuronal structures exert a ‘soothing touch’ to dampen excitability in pathological conditions (Badimon et al., 2020; Cserép et al., 2020; Eyo et al., 2014; Kato et al., 2016; Li et al., 2012; Merlini et al., 2021; Szalay et al., 2016; Wake et al., 2009). We tested whether microglia were protective in edema by quantifying neuronal death in a microglia depletion model. CX3CR1$^{EGFP/+}$ mice were fed chow containing the colony-stimulating factor 1 receptor (CSF1R) inhibitor PLX3397 (PLX), which robustly and selectively depletes microglia throughout the brain (Elmore et al., 2014). We quantified microglia density in 3-dimensional cortical volumes with 2-photon imaging and found a ~78% reduction in microglial numbers in mice fed PLX chow compared to the control diet after at least 21 days (Fig. 6a,b), as previously reported (Elmore et al. 2014). Examination of slices from PLX-treated versus control-diet mice revealed significant increases in veratridine-induced PI loading in neurons when microglia

were depleted (Fig. 6a,c). These data suggest a protective role for microglia to reduce neuronal death during swelling.

If microglia contacts are protective in cytotoxic edema, then inhibiting $P2Y_{12}R$ to prevent ATP-dependent microglia attraction to swollen neurons should exacerbate cell death. We therefore repeated the veratridine-PI loading experiments in $CX3CR1^{EGFP/+}$ mice with normal microglia populations (i.e. no PLX) with and without the specific $P2Y_{12}R$ inhibitor PSB-0739 (PSB, 5 μM), and found a significant increase in cell death when $P2Y_{12}R$ was blocked (Fig. 6d,f). Consistent with this, we observed a proportional reduction in PI-positive neurons enwrapped by microglia processes in PSB treated tissue (Fig. 5e,g), indicating $P2Y_{12}R$ signaling in microglia is critical in the formation of microglia-neuron contacts (Eyo et al., 2014; Umpierre and Wu, 2021). Together, these data show that protective microglia contacts in edema require ATP-chemotaxis transduced via neuronal Panx1 and microglia $P2Y_{12}R$.

Discussion

We conclude, based on several lines of evidence, that swelling-induced neuronal death is precipitated by ROS-dependent Panx1 opening, which in turn triggers ATP release to attract protective microglia contacts (Fig 7). First, the initial phase of death during cytotoxic edema was inhibited by Panx1 blockers and was significantly reduced in $Panx1^{-/-}$ transgenic mice compared to wild type. Second, neuronal swelling by veratridine application induced intense oxidative stress and lipid peroxidation that was due to swelling itself because these changes were not observed in low$[Cl^-]_o$. Third, oxidative stress triggered Panx1 currents in patch-clamped hippocampal neurons that was sensitive to ROS scavengers and Panx1 inhibitors. Last, we show ATP release through Panx1 leads to increased microglia contacts, indicating that although Panx1 opening in neuronal swelling is initially detrimental, it also provides protective feedback at the tissue level by mobilizing protective microglia.

Cytotoxic neuronal swelling is a hallmark of stroke and TBI (Donkin and Vink, 2010; Simard et al., 2007). By both imaging PI dye uptake and measuring LDH release we show that swelling itself is sufficient to cause neuronal death (Rungta et al., 2015) via Panx1 opening. This death pathway is distinct from glutamate excitotoxicity and apoptosis because it occurs independent of Ca^{2+} influx and is initially reversible (Choi, 1987; Dreier et al., 2018; Gottron et al., 1997; Rungta et al., 2015). Indeed, our present and previous work shows that death in edema will occur even if canonical pathways, such as NMDAR- and voltage-gated Ca^{2+} channel Ca^{2+} influx, are blocked or in Ca^{2+}-free ACSF (Rungta et al., 2015). ROS-Panx1 opening described here is therefore independent of the previously described NMDAR-Panx1 signaling in ischemia (Thompson et al., 2008; Weilinger et al., 2016). Although these death pathways are distinct, it is likely that ROS- and NMDA-Src-signaling cascades both contribute to neuronal dysfunction when glutamate excitotoxicity and swelling converge in ischemia. Future work assessing the role of Panx1 in the post-ischemic brain will be pivotal to clarify how cell death occurs in edema that can persist long after reperfusion (Liang et al., 2007; Simard et al., 2007).

Although Panx1 has been reported to be mechanosensitive in erythrocytes, recent work indicates that Panx1 opening in mechanical stress is downstream of mechanosensitive Piezo1 channel activation (Desplat et al., 2021; Diem et al., 2020). The data presented here suggest that Panx1 is not opened by swelling directly, and instead requires swelling-induced ROS generation. We saw dramatic reductions in veratridine-triggered lipid peroxidation and roGFP1 oxidation in low$[Cl^-]_o$ conditions, suggesting the trigger for ROS is not Na^+/K^+ dysregulation but swelling itself. Neuronal membrane stretch can cause mitochondrial dysfunction and oxidative stress in *in vitro* models of TBI (Ahmed et al., 2000; Arundine et al., 2004; Ji et al., 2012; Shah et al., 1997). While not osmotic swelling *per se*, these studies found that increasing cell size using transient pressure insults generated ROS (Arundine et al., 2004; Ji et al., 2012). Mechanosensitive ROS formation can also occur directly via NADPH Oxidase (Nox) pathways in vascular epithelial cells (Brandes et al., 2014) and swollen astrocytes (Reinehr et al., 2007). Panx1-Nox coupling has been suggested in inflammatory bowel disease, chronic obstructive pulmonary disease, and cardiovascular diseases (Hung et al., 2013; Xu et al., 2018), but this occurs downstream of Panx1 opening, requiring ATP release and purinergic receptor activation (Xu et al., 2018). Although the source of ROS is uncertain, our data provide direct evidence of cytoplasmic oxidation in neurons during swelling by roGPF1 imaging, lipid peroxidation, and reductions in neuronal AA concentration.

To our knowledge, the present study provides the first confirmation *in situ* that cytosolic oxidation opens Panx1 channels. Though the precise mechanism linking ROS generation and Panx1 activation during swelling is unknown, it could involve direct or indirect regulation. Panx1 contains redox-sensitive cysteine residues in critical regions such as the c-terminus, its extracellular and intracellular loops, and within the pore-forming domains (Bunse et al., 2009; Bunse et al., 2011; Bunse et al., 2010; Onami et al., 2014; Wang and Dahl, 2010), indicating the channel could be opened directly by ROS. Indeed, cysteines on the c-terminal (C426 and C346) and inner vestibule (C40) are important for basal inhibition and are conserved from rodents to human (Boyce et al., 2018; Sandilos et al., 2012; Wang and Dahl, 2010). Physiological ‘ball and chain’ gating is thought to occur through dissociative uncoupling of disulfide bonds between c-terminal cysteines and pore-lining residues (Chekeni et al., 2010; Sandilos et al., 2012; Wang and Dahl, 2010). Application of reducing agents in oocyte or HEK293 expression systems also inhibits currents in recombinant Panx1 (Bunse et al., 2009; Bunse et al., 2010), further suggesting the protein is directly modified by redox changes. However, given that Panx1 is also controlled by phosphorylation state, indirect channel activation via ROS-sensitive kinases might also play a role (Giannoni et al., 2005; Lohman et al., 2019; Weilinger et al., 2016; Weilinger et al., 2012).

Our direct ATP efflux measurements in swelling that was reduced in the $Panx1^{-/-}$ mouse indicate Panx1 is a key conduit for ATP release (Chekeni et al., 2010; Sandilos et al., 2012). We observed a dramatic reduction in $P2Y_{12}R$-mediated microglia contacts on neurons when Panx1 was blocked using the specific peptide inhibitor ^{10}panx, further supporting a Panx1-ATP-microglia signaling axis. This is consistent with the first demonstration of protective microglia contacts in zebrafish that required Panx1-mediated ATP release from neurons (Li et al., 2012). Somatic ATP release via vesicular exocytosis could also signal to microglia

(Zhang et al., 2007), which have been shown to form specialized microglia-neuron junctions (Cserép et al., 2020). While we cannot exclude a role for vesicular ATP release in our swelling model, the ^{10}panx inhibitor reduced the rate of new microglia-neuron contacts to control levels. We also observed frequent contacts under physiological conditions which could be due to vesicular ATP release and long lasting intercellular junctions (Cserép et al., 2020; Zhang et al., 2007).

The present findings also support a protective role for microglia-neuron contacts in cytotoxic edema. Neuronal death in edema was significantly increased when microglia were depleted in our PLX model, or when $P2Y_{12}R$-dependent chemotaxis was pharmacologically blocked with PSB, indicating that the presence of microglia, and their capacity to contact neurons, is neuroprotective. Indeed, microglia contacts are thought to exert important homeostatic control by dampening activity in hyper-excitable neurons (Kato et al., 2016; Li et al., 2012), which has been extended to disease models such as epilepsies (Badimon et al., 2020; Eyo et al., 2014; Merlini et al., 2021), and stroke (Cserép et al., 2020; Szalay et al., 2016; Wake et al., 2009). Although the mechanism for neuroprotection by microglia contacts are not fully understood, possibilities include (i) local ATP catabolism by microglia suppresses neuronal excitability via adenosine receptor (A_1R) signaling (Badimon et al., 2020), (ii) extracellular K^+ buffering (Mapps et al., 2022), and (iii) G_i-driven activity in microglia. Future work exploring the protective mechanism of microglia contacts will be vital to identify novel therapeutic targets, particularly in ischemia and other pathologies where ATP levels are perturbed.

In conclusion, we have elucidated a double-edged role for Panx1 in neuronal death and protection pathway intrinsic to swelling. On one hand, the data presented here suggest that inhibitors of Panx1 channels or ROS generation may be novel therapeutic avenues for cytotoxic edema and could reduce the high rate of neurological disability in survivors of TBI or stroke (Rieke et al., 1995). On the other hand, long-term Panx1 inhibition might be detrimental by attenuating protective microglia contacts. Considering this divergent role for Panx1 in cytotoxic edema, together with demonstrations in other pathologies (Dossi et al., 2018; Giaume et al., 2019; Karatas et al., 2013; Thompson et al., 2006), future work assessing the temporal relationship between Panx1-mediated death and protective ATP release in disease would be necessary if Panx1 is to be explored as a therapeutic target.

Limitations of the Study

The present work uses a combination of pharmacological and genetic knockdown approaches to demonstrate the cytotoxic, and protective, roles of Panx1 opening in edema. One limitation – and a challenge for any Panx1 study – is off-target effects of most Panx1 inhibitors (Koval et al., 2023). For example, CBX also blocks connexin channels whereas probenecid is an agonist for Transient receptor potential vanilloid 2 (TRPV2) channels and an antagonist for solute transporters (Bang et al., 2007a; Koval et al., 2023). To address this challenge, our study was designed to use the specific peptide inhibitor ^{10}panx, and its scrambled control (^{SC}panx), wherever possible. In addition, most experiments were repeated using different Panx1 blockers (e.g. CBX and/or probenecid) to further support our ^{10}panx data and provide redundancy to account for nonspecific pharmacology.

Although not statistically comparable, our data suggest that pharmacological Panx1 block (rat) was more effective than the Panx1$^{-/-}$ model (mouse) in reducing neuronal death in edema as measured by LDH release (Fig 1gh). Aside from potential species variations, one possible explanation for this difference is compensation by other pannexin isoforms (e.g. Panx2 and/or Panx3). For example, Panx3 is upregulated in neurons of constitutive Panx1$^{-/-}$ animals in the vomeronasal organ *in vivo* and Neuro2a cells *in vitro* (Whyte-Fagundes et al., 2018), vasculature (Lohman et al., 2012a), and skin (Penuela et al., 2014), and forms functional ATP release- and dye-uptake channels (Whyte-Fagundes et al., 2018). Similarly, compensation by Panx2 channels has been suggested in a rat *in vivo* stroke study (Bargiotas et al., 2012). Notwithstanding the possibility of partial Panx1 compensation by other proteins, our data from Panx1$^{-/-}$ animals are consistent with our rigorous pharmacology experiments, together supporting the role for Panx1 opening in edema.

Materials and Methods

Animals

Animal care protocols were approved by the University of British Columbia, the Mayo Clinic, and Rutgers University Animal Care Committee in compliance with the Canadian Council on Animal Care guidelines. All animals were housed on a 12:12 hour light:dark cycle with *ad libidum* access to laboratory chow. Experiments in rat were performed in male animals, and both males/females were used in mouse experiments. Panx1$^{-/-}$ and Panx1^{WT} mice were age-matched C57BL/6 from Genentech as described (Qu et al., 2011) and were kindly provided with permission by Dr. Dale W. Laird (University of Western Ontario, Canada). CX3CR1$^{EGFP/+}$ animals from Jackson Lab (strain 005582) were crossbred with C57BL/6 (WT) mice. For P2Y$_{12}$R$^{-/-}$ experiments, CX3CR1$^{GFP/+}$ P2Y$_{12}$R$^{-/-}$ mice were generated by crossbreeding CX3CR1$^{GFP/+}$ mice with P2Y$_{12}$R$^{-/-}$ mice and again crossbreeding the offspring with P2Y$_{12}$R$^{-/-}$. Genotyping was performed from ear lobe tissue (Transnetyx Inc). Sprague Dawley (SD) rats were from Charles River.

Acute Slice Preparation

SD rats or WT/transgenic mice (P17–25 unless otherwise indicated) were anesthetized by isoflurane inhalation in air and decapitated; the brain was sliced while submerged in an ice-cold solution consisting of (in mM): 120 NMDG, 2.5 KCl, 25 $NaHCO_3$, 1 $CaCl_2$, 7 $MgCl_2$, 1.2 NaH_2PO_4, 20 glucose, 2.4 Na-pyruvate, 1.3 Na-ascorbate, and saturated with 95% O_2/5% CO_2 with a pH of 7.3–7.4. Transverse or coronal slices were cut (370–400 μm for rat, 300 μm for mice) and transferred into a chamber containing artificial cerebrospinal fluid (ACSF) at 32°C for one hour prior to experimentation. ACSF consisted of (in mM): 120 NaCl, 25 $NaHCO_3$, 3 KCl, 1.25 NaH_2PO_4, 2 $MgCl_2$, 2 $CaCl_2$, and 10 glucose and was saturated with 95% O_2/5% CO_2 (pH of 7.3–7.4). Low Cl^- conditions were achieved by substituting NaCl with NaGluconate in the ACSF.

Chemicals and Reagents

Drugs and dyes used for experiments are listed in final concentration (in mM) and were purchased from the following suppliers: 0.05 D-APV, 0.01 CNQX, 1 DIDS (Tocris), 0.05 veratridine (Tocris and Abcam), 0.1 ^{10}panx (WRQAAFVDSY) and 0.1 ^{SC}panx

(FSVYWAQADR) were either generously synthesized and provided by Dr. Yu Tian Wang (University of British Columbia, Canada), were gifted from Dr. Roger Thompson (University of Calgary, Canada), or were synthesized by New England Peptide. 1 L-ascorbate, 5 N-acetyl-L-cysteine (Chao et al., 2016), 0.1 trolox (Vaarmann et al., 2010), 0.1 carbenoxolone, 8 H_2O_2, 1 probenecid, 0.05 picrotoxin, 0.02–0.04 propidium iodide, 0.001 SR101, xanthine (20 μg/mL), clotrimazole (0.01), ruthenium red (0.01) and salts for ACSF and slicing solution were from Sigma-Aldrich. Xanthine oxidase (25 μg/mL) was from EMD Millipore, and 0.1 Alexa-350 and 0.05 Alexa-594 hydrazide was from Thermo Fisher Scientific. Z-VAD (0.1) was from R&D Systems Inc. All drugs were made into aliquots dissolved in water or DMSO and diluted to the final concentration in ACSF or intracellular recording solution. The final concentration of DMSO never exceeded 0.1% v/v unless stated otherwise.

Primary antibodies used for Western blotting were: 1/1000 Panx1 CT395 (Penuela et al., 2009) or 1/1000 Panx1 (D9M1Cl, Cell Signaling Technology); 1/300 Transferrin Receptor (Zymed); 1/100–1/200 Cleaved Caspase-3 (Cell Signaling Technology); 1/4000 Actin (Santa Cruz Biotechnology). Secondary antibodies used were: 1/2000 horseradish peroxidase (HRP)-conjugated donkey anti-rabbit; 1/2000 HRP-conjugated donkey anti-mouse; 1/2000 HRP-conjugated donkey anti-goat (all from Jackson Immunoresearch).

Lactate dehydrogenase release assay

LDH assay kits (Biomedical Research Service Center, State University of New York at Buffalo) were used to investigate cell death using rat hippocampal slices. Transverse hippocampal/cortical slices were pre-treated with a cocktail of inhibitors (PTX, CNQX, D-APV) for 30 min prior to application of veratridine (15 min) in a 6 well plate aerated with 95% O_2/5% CO_2 at 32°C on an insert for organotypic culture (Millipore). After veratridine exposure, slices were transferred to another incubation chamber for 90 min at 32°C. Supernatants were collected at 90 min and then slices were lysed using lysis buffer. The LDH level in the supernatant represents the cell death, whereas the LDH level in lysed cells represents the viable cells. In brief, supernatants and cell lysates were centrifuged for 3 min at 16,000*g* at 4°C. Samples were added into a 96-well plate with LDH assay solution and incubated for 30 min at 37°C and then acetic acid (3%) was added to stop the reaction. LDH reduces tetrazolium salt INT to formazan, which is water-soluble and exhibits an absorption maximum at 492 nm. Absorbance was measured at 492 nm using a microplate reader. Cell death was presented as percentage of released LDH compared to cell lysate LDH.

Lipid Peroxidation

Lipid peroxidation assay kit (Biomedical Research Service Center, State University of New York at Buffalo) was used to measure oxidative stress in rat brain slices (Zhang et al., 2014). In brief, malondialdehyde (MDA), the most abundant lipid peroxidation product, was measured after the samples were treated with 2-thiobarbituric acid (TBA). Slices were treated with veratridine for 15 min then transferred to an incubation chamber then collected for the analysis. Slices were also treated with X/XO for two hours for the lipid peroxidation assay. Trichloroacetic acid (TCA, 10% v/v) solution was used to homogenize the slices

after treatment. The homogenates were mixed with TBA solution with 1:1 ratio then heated at 95 °C for 30 min. The samples were mixed vigorously with n-butanol. Subsequently the samples were centrifuged at 13000*g* for 5 min. The supernatants were collected and the absorbance was measured at 532 nm. Lipid peroxidation levels were measured and normalized with the protein levels of the samples.

Ascorbate measurements

Ascorbate assay kit (Sigma-Aldrich) was used to measure the concentrations of ascorbate in the tissue in the presence or absence of veratridine. In brief, brain slices were collected at different time points then rapidly homogenized in cold buffer and centrifuged at 13,000*g* at 4 °C to eliminate insoluble debris. Fe^{3+} is reduced to Fe^{2+} in the presence of antioxidants including ascorbate. Ascorbate oxidase is used to oxidize any ascorbic acid in the sample to measure the concentration of ascorbate. The absorbance was measured at 570 nm. Ascorbate levels were normalized with the protein levels of the samples.

Slice swelling imaging assay

Slices were transferred to a 24-well plate aerated with 95% O_2/5% CO_2 into homemade 3D-printed inserts with mesh bottoms for ambient aeration. Temperature was consistently maintained at 32 °C by perfusing heated water between wells. Swelling was induced by continuous veratridine application. We used an in-house apparatus to measure swelling based on a Raspberry Pi single board computer (model 2b) and camera. Images were acquired every 5 seconds and were analyzed using an automated custom MATLAB script.

Propidium iodide loading and imaging

Acute cortical slices from rat were pre-incubated in 20 μM propidium iodide (PI) and D-APV, picrotoxin, CNQX for 30 minutes, as well as specified pannexin inhibitors. NAC and trolox were pre-incubated for at least 1 hour prior to veratridine exposure. Slices were exposed to veratridine for 15 minutes followed by flash fixation at different time points by the SNAPSHOT method described previously (Dissing-Olesen and MacVicar, 2015). Briefly, slices were fixed in PFA at 80°C for 2 minutes and then washed in 0.1 M PBS. Slices were then permeabilized for 1–2 weeks in a 0.1 M PBS solution containing 2% v/v Triton X-100 and 20% v/v final DMSO at 4°C to improve tissue transparency for PI imaging.

Fixed slices were imaged using a Zeiss LSM 7MP 2-photon laser scanning microscope and a Ti:Sapphire Chameleon Ultra II laser (Coherent) tuned to 900 nm for better tissue penetration. Optical sections of cortical layers 4–6 were acquired at 512 × 512 pixels (imaging area 425.1 × 425.1 μm) through the entire tissue depth (370–400 μm). Imaging analysis in cortical layers allowed for accurate PI uptake quantifications where neuronal density is low (compared to dense cell body layers in the hippocampus). PI staining analysis was conducted over 100 μm from the slice center (e.g. 200 μm ± 50 μm for a 400 μm thick slice) due to an expected pattern of staining close (<70 μm) to the slice surface due to shear injury from preparing brain slices (Bak et al., 1980; Dzhala et al., 2012). Image stacks were thresholded in Fiji (ImageJ) using built-in Otsu thresholding, and neurons were identified

based on size and circularity using the ‘analyze particles’ function. PI positive cell density was calculated as ρ = #cells / volume.

AAV injection

roGFP1 expression was induced by an AAV-CBA-roGFP1-WPRE construct which we reproduced and adapted from (Xie et al., 2013) using the serotype AAV9. Similarly, EGFP was expressed using AAV9-Thy1-EGFP using the AAV9 serotype (Canadian Neurophotonics Viral Vector facility). Neonatal rats (P2–3) were anesthetized with isoflurane and 2 μL of virus containing solution was injected stereotactically into the lateral ventricles. The animals were allowed to recover and used for experiments at the age of P18–25.

Two-photon imaging of roGFP1

Acute coronal brain slices from AAV-roGFP1 injected animals were incubated in ACSF containing SR101 during slice recovery. Brain slices were transferred to a static chamber inside the microscope in 2–3 mL ACSF containing D-APV, CNQX and picrotoxin and was continuously gassed with 95 % O_2/ 5 % CO_2. For a subset of experiments low$[Cl^-]_o$ ACSF was used together with DIDS (final DMSO concentration 0.2%). All experiments were performed at room temperature. Cortical neurons from layer IV to VI were imaged 50 to 80 μm deep. Excitation wavelengths of 740 and 910 nm were used alternately in a time series to excite roGFP1 and the green fluorescence was recording from 500 to 550 nm. Veratridine, H_2O_2, or control ACSF were puffed onto the slice surface using borosilicate glass pipettes with 0.5 to 0.8 psi lateral (minimum 20 μm) to the region of interest.

For data analysis we identified roGFP1 positive neurons as region of interests and calculated the emission ratios after excitation of 740 nm and 910 nm. Ratios were normalized to their respective baselines and were adjusted to a linear regression curve calculated from the individual baselines. Neurons were considered to be responding (i.e. being oxidized) to either veratridine or H_2O_2 if the average fluorescent intensities during drug application was greater than two times the standard deviation of the respective averaged intensities of control ACSF puffs.

Acutely isolated hippocampal CA1 neurons and whole-cell recordings

Hippocampal CA1 neurons were isolated from SD rats (P14–22). Following anesthetization and decapitation, the brain was rapidly transferred to oxygenated (with 95% O_2/ 5% CO_2) ACSF. The hippocampus was rapidly isolated and transverse slices were cut by hand. Then slices were stored in oxygenated ACSF at room temperature for 45 minutes, after which papain (25 mg) was added to digest slices for 30 minutes. Slices were then washed three times in fresh ACSF and allowed to recover in oxygenated ACSF at room temperature (20–22°C) for two hours before use. Before the recording, slices were transferred to a 35 mm petri dish and placed under a microscope. Fine tip forceps were used to dissociate hippocampal neurons by gently taping the slices.

Tight seal whole-cell voltage-clamp recordings were performed on acutely dissociated neurons using glass recording electrodes (resistances of 3–5 MΩ) pulled from borosilicate

glass (1.5 μm diameter, WPI) and filled with intracellular solution that contained (in mM): 100 Cs-methanesulfonate, 5 NaCl, 25 CsCl, 5 4Cs-BAPTA, 20 HEPES, 5 tetraethylammonium (TEA), and 2 MgATP, pH 7.2 (osmolarity between 290 and 300 mOsm). Neurons were constantly perfused with normal ACSF solution plus a cocktail of blockers including (in mM): 10 TEA, 1 4-AP, 1 Kynurenic acid, 0.05 $CdCl_2$, 0.01 nifedipine and 0.001 TTX. Briefly, after the formation of a tight seal (>1 GΩ), negative pressure was used to rupture the membrane and gain whole cell access. Once achieved, neurons were voltage clamped at −60 mV and 150 ms ramps between −60 and +60 mV were applied every 10 s. When series resistance varied more than 15 MΩ, the cell was discarded. Drugs were included in the patch pipette or in the bath. Recordings were conducted at room temperature (20–22°C). Baseline and peak holding currents were taken at the first and last minutes of the recording, respectively, and recordings were held for 10 or 15 minutes. Currents were recorded using MultiClamp 700B amplifiers (Axon Instruments, Union City, CA), and data were filtered at 2 kHz and acquired using Clampex (Axon Instruments).

Whole-cell patch clamp and hypertonic swelling in acute cortical slices

Whole-cell voltage-clamp recordings were made from pyramidal neurons in acutely prepared cortical brain slices (400 μm thick). During recordings, brain slices were perfused with 95% O_2/ 5% CO_2 bubbled ACSF (32°C, 300 mOsm) containing (in mM): 0.0005 TTX, 0.05 $CdCl_2$, 0.04 propidium iodide. To test for pannexin-1 involvement, brain slices were incubated in the ACSF drug cocktail supplemented with either ^{SC}panx (100 μM) or ^{10}panx (100 μM) peptide. For experiments, neurons were dialyzed with internal solution of regular osmolarity (290 mOsm) or high osmolarity (380–400 mOsm) via a patch pipette (resistance 2–3 MΩ). The regular osmolarity internal solution was composed of (in mM): 108 Cs-methanesulfonate, 8 TEACl, 8 Na-Gluconate, 1 EGTA, 4 K-ATP, 0.3 NaGTP, 10 HEPES, 2 $MgCl_2$, and 0.1 Alexa Fluor 350 hydrazide. The high osmolarity internal was made with further addition of Cs-methanesulfonate to bring the solution osmolarity to 380 mOsm. Internal solution pH was set to 7.2 by addition of Cs-hydroxide (Sigma-Aldrich). Neuronal membrane current at −80 mV was measured under voltage-clamp using a MultiClamp 700B amplifier and digitized with a DigiData 1440A analog-to-digital converter and the Clampex acquisition program of pClamp software (Axon Instruments). Neuronal size and propidium iodide loading were visualized using a two-photon laser scanning microscope (Zeiss LSM 7MP) with a Zeiss 20x W/1.0 NA objective coupled to a Coherent Chameleon Ultra II laser to produce excitation light at 750 nm. Images (512 × 200 pixels) for time-lapse analysis were collected at 0.2 Hz using 8-line averaging. Emitted light from Alexa Fluor 350 and propidium iodide was split at 560 nm by a dichroic mirror before being passed through blue (Chroma, 460/50 M) and red emission filters (Chroma, 630/75 M-2P) respectively. Emitted blue and red light was then detected using two separate Zeiss Binary GaAsP detectors.

Neuronal swelling experiments in $P2Y_{12}R^{-/-}$ mice

For the hypotonic bath model, the ACSF was switched from baseline (in mM): 124 NaCl, 25 $NaHCO_3$, 2 KCl, 1 KH_2PO_4, 2 $CaCl_2$, 2 $MgSO_4$, 10 glucose, and sucrose added to make 300–320 mOsm to a hypotonic ACSF: 85 NaCl, 25 $NaHCO_3$, 2 KCl, 1 KH_2PO_4, 2 $CaCl_2$, 2 $MgSO_4$, 10glucose, to make ~190–200 mOsm. For single cell swelling, neurons were patch loaded with a hypertonic intracellular solution containing (in mM): 120 KGluc, 5 NaCl, 0.2

EGTA, 10 HEPES, 1 $MgCl_2$, 2 MgATP, 0.3 Na_2GTP, 10 Na_2phosphocreatinine, and Alexa Fluor dye 594 (Life Technologies). pH was adjusted 7.25 using NaOH, and the osmolarity was adjusted with sucrose solution (10M) to achieve ~ 400 mOsm.

Quantification of microglial process convergence (MPC) events was done manually from 330 × 330 × 45 μm fields-of-view for 40 min recordings of brain slices. Data are presented as mean ± SEM. Student's t test or one-way ANOVA with Bonferroni corrections were used to establish significance.

Microglia-neuron contact imaging and analysis

Swelling in individual patched neurons was performed as described above, with the addition of Alexa-594 hydrazide (50 μM) to monitor somatic swelling. Neurons were patched from $CX3CR1^{EGFP/+}$ mice to simultaneously monitor swelling and EGFP-expressing microglia processes. Alexa594 and EGFP were excited by 2-photon laser tuned to 920 nm. Fluorescence emission was detected with a photo-multiplier tube after passing through a 490–550 nm emission filter (Chroma, ET520/60m) fitted on a Zeiss LSM 7MP as described above. 3-dimensional XYZ time series were collected by acquiring 10–35 Z-frames spanning 33–132 μm depth, centre-focused on neuronal somata. Microglia-neuron contacts were manually counted according to the following criteria: i) process must not be transitory to pipette, ii) must be on the soma, iii) must be a new contact after whole-cell break-in, iv) must be static for at least two time points, v) process must extend to soma (i.e. neuron soma swelling into a static process from a satellite microglia does not count), vi) only contacts made by microglia process tips were counted. To normalize for varying recording times, microglia contact rate was calculated by dividing the total contacts by the recording duration.

Microglia depletion with PLX3397

PLX3397 was purchased from MedChemExpress and was then incorporated into AIN76A chow at 290 mg/kg by Research Diets, Inc. $CX3CR1^{EGFP/+}$ mice were fed a special diet containing either PLX3397 chow or AIN76A control chow for at least 3 weeks prior to imaging similar to a previous report (Elmore et al., 2014). Experiments were performed on age-matched pairs of control and PLX diet animals daily to control for possible variations in depletion efficacy after the 3-week mark.

Microglia surveillance analysis and laser lesion model

Microglia from $CX3CR1^{EGFP/+}$ mice were imaged in the stratum radiatum of the CA1 region at 150 ± 25 μm below the surface of the slice. Images for time-lapse analysis were collected at 512 × 512 pixels using 8-line averaging. Time series of image stacks of 30 μm depth with a step size of 2 μm in the z-axis, at a rate of 1 stack per minute. Lesions were induced by exposure of high laser power illumination to a restricted area.

For microglial motility index quantification, microglia were imaged every minute, z-stacks were aligned and projected stack images were binarized. The number of new pixels (additions) at each time point was normalized to the total number of pixels in the cells (cell size), therefore giving a quantification of motility normalized to cell size.

Western Blotting

Wild-type and Panx1$^{-/-}$ cortical tissue was collected from P15 mice and homogenized on ice in RIPA buffer (Tris Buffered Saline [TBS] with 1% IGEPAL, 0.5% sodium deoxycholate, 0.1% SDS) supplemented with complete ULTRA protease inhibitor cocktail (Sigma-Aldrich), phosSTOP phosphatase inhibitors (Roche), and 1 mM EDTA. Homogenates were passed three times through a 27-gauge syringe, incubated on ice for 60 minutes and then centrifuged at 4 °C for 20 minutes at 12,000 rpm to remove debris. Protein concentration was determined using a DC Protein Assay (Bio-Rad), and equal protein amounts were heated at 95 °C for 5 minutes in Laemmli Sample buffer under reducing conditions (5% β-mercaptoethanol) before loading onto gels. Gels were transferred to 0.2 μm pore-size polyvinyldene fluoride (PVDF) membrane using a Trans-Blot Turbo semi-dry transfer system (Bio-Rad). Blocking and antibody incubations took place in blocking buffer (5% skim milk in TBS with 0.1% Tween 20). Blots were imaged using a C-DiGit western blot scanner (LI-COR).

For activated caspase-3 analyses, acute slices were obtained from P14–21 SD rat pups. Slices were recovered for 30 minutes in ACSF at 32°C with bubbling. Slices were then transferred to treatment solutions at 32°C with bubbling: 50 μM veratridine or control ACSF for one and two hours, or 25 μM raptinal (rapid apoptosis inducer) for two hours (Heimer et al., 2019; Palchaudhuri et al., 2015). Slices were collected, lysed in RIPA buffer, and analyzed by Western botting, as written above.

Cell Surface Biotinylation

Acute slices were obtained from P14–21 SD rat pups. Slices were recovered for 60 minutes in ACSF at 32 °C with bubbling, then transferred to treatment solutions for one hour at 32°C with bubbling: Control ACSF; ACSF + 50 μM veratridine for 15 min, then 45 minutes in Control ACSF; ACSF + 20 μg/mL xanthine; ACSF + 20 μg/mL xanthine + 2.7 μL/mL xanthine oxidase. After one hour, slices were transferred into ice-cold ACSF + 1 mg/mL EZ-link NHS-SS-biotin (Thermo Scientific) for 15 minutes. Slices were washed once with ice-cold Quench Buffer (ACSF + 100 mM glycine), then incubated for 15 minutes in Quench Buffer. Slices were lysed in RIPA buffer as written above. Equal amounts of protein lysates (500 μg) were incubated overnight with 50 μL of streptavidin agarose beads (Thermo Scientific). Beads were washed three times with TRIS-lysis buffer (150 mM NaCl, 10 mM TRIS–HCl, pH 7.4, 1 mM EDTA, 0.5% IGEPAL, and 1% Triton X-100) and once with TBS, then resuspended in Laemmli sample buffer under reducing conditions (5% β-mercaptoethanol) and incubated at 95°C for 10 min. Samples were analyzed by SDS–PAGE and Western blot in parallel with 15 μg of total protein lysate (input) as written above. Blots were imaged using a Bio-Rad Chemi-Doc.

QUANTIFICATION AND STATISTICAL ANALYSIS

Data processing and analysis was performed in Excel (Microsoft) and Prism 6 or 7 (GraphPad). Statistical analyses were performed in Prism and individual tests for each experiment are described in the figure legends. Statistical significance was determined using corresponding statistical tests and reported as either exact p value or: ‘n.s.’= $p>0.05$,

*p<0.05, **p<0.01, ***p<0.001, ****p<0.0001. Experimental replicates (n) are stated directly in the figures and/or figure legends. Student's paired and unpaired t-tests (two-tailed) were used to compare means between two datasets. One-way ANOVA with Tukey's multiple comparison test was used for datasets with three or more groups. Data are presented as mean + SEM in all figures.

Supplementary Material

Refer to Web version on PubMed Central for supplementary material.

Acknowledgements:

The authors thank Holden Beggs for his programming of the user interface for the slice swelling assay. The authors declare no competing interests. roGFP1 plasmids were a generous gift from Brian Bacskai and roGFP1 and EGFP plasmids were packaged into AAV by the Canadian Neurophotonics Platform Viral Vector Core Facility (RRID:SCR_016477, (Université Laval, QC, Canada). ^{10}panx and ^{SC}panx were either synthesized and provided by Dr. Yu Tian Wang's Peptide Synthesis Facility (University of British Columbia, Canada) or was generously gifted by Dr. Roger Thompson (University of Calgary, Canada). Panx1 KO mice were kindly provided by Dr. Dale W. Laird (University of Western Ontario, Canada). This work was supported by resources and personnel (J.L.) made available through the NeuroImaging and NeuroComputation Centre at the Djavad Mowafaghian Centre for Brain Health (RRID: SCR_019086).

Funding:

This project was funded by the Canadian Institutes of Health Research (CIHR) #FDN148397, funding from the Fondation Leducq Network grant #15CVD-02 and previous CIHR # 245760 to B.A.M. and CIHR #10677 to T.P.S., National Institutes of Health R01NS088627 to L.J.W. and the Koerner Foundation (T.P.S, B.A.M.), CIHR postdoctoral fellowship (C.J.G. and L.E.W.S), and Banting fellowship grants (N.L.W.), as well as MSFHR (N.L.W., C.J.G., L.W.S.), and Killam fellowships (L.W.S.). B.A.M. was supported by a Canada Research Chair in Neuroscience and TPS as the Canada Research Chair in Biotechnology and Genomics-Neurobiology.

References

Ahmed SM, Rzigalinski BA, Willoughby KA, Sitterding HA, and Ellis EF (2000). Stretch-induced injury alters mitochondrial membrane potential and cellular ATP in cultured astrocytes and neurons. Journal of neurochemistry 74, 1951–1960. [PubMed: 10800938]

Angelova PR, and Abramov AY (2018). Role of mitochondrial ROS in the brain: from physiology to neurodegeneration. FEBS Lett 592, 692–702. [PubMed: 29292494]

Arundine M, Aarts M, Lau A, and Tymianski M (2004). Vulnerability of central neurons to secondary insults after in vitro mechanical stretch. The Journal of neuroscience : the official journal of the Society for Neuroscience 24, 8106–8123.

Badimon A, Strasburger HJ, Ayata P, Chen X, Nair A, Ikegami A, Hwang P, Chan AT, Graves SM, Uweru JO, et al. (2020). Negative feedback control of neuronal activity by microglia. Nature 586, 417–423. [PubMed: 32999463]

Bak IJ, Misgeld U, Weiler M, and Morgan E (1980). The preservation of nerve cells in rat neostriatal slices maintained in vitro: a morphological study. Brain research 197, 341–353. [PubMed: 6250666]

Bang S, Kim KY, Yoo S, Lee S-H, and Hwang SW (2007a). Transient receptor potential V2 expressed in sensory neurons is activated by probenecid. Neuroscience letters 425, 120–125. [PubMed: 17850966]

Bang S, Kim KY, Yoo S, Lee SH, and Hwang SW (2007b). Transient receptor potential V2 expressed in sensory neurons is activated by probenecid. Neurosci Lett 425, 120–125. [PubMed: 17850966]

Bargiotas P, Krenz A, Monyer H, and Schwaninger M (2012). Functional outcome of pannexin-deficient mice after cerebral ischemia. Channels (Austin) 6, 453–456. [PubMed: 23111424]

Bialecki J, Werner A, Weilinger NL, Tucker CM, Vecchiarelli HA, Egana J, Mendizabal-Zubiaga J, Grandes P, Hill MN, and Thompson RJ (2019). Suppression of Presynaptic Glutamate

Release by Postsynaptic Metabotropic NMDA Receptor Signalling to Pannexin-1. The Journal of neuroscience : the official journal of the Society for Neuroscience.

Bolaños JP (2016). Bioenergetics and redox adaptations of astrocytes to neuronal activity. Journal of neurochemistry 139, 115–125. [PubMed: 26968531]

Boyce AKJ, Epp AL, Nagarajan A, and Swayne LA (2018). Transcriptional and post-translational regulation of pannexins. Biochim Biophys Acta Biomembr 1860, 72–82. [PubMed: 28279657]

Brandes RP, Weissmann N, and Schroder K (2014). Nox family NADPH oxidases in mechano-transduction: mechanisms and consequences. Antioxidants & redox signaling 20, 887–898. [PubMed: 23682993]

Bunse S, Locovei S, Schmidt M, Qiu F, Zoidl G, Dahl G, and Dermietzel R (2009). The potassium channel subunit Kvbeta3 interacts with pannexin 1 and attenuates its sensitivity to changes in redox potentials. FEBS J 276, 6258–6270. [PubMed: 19780818]

Bunse S, Schmidt M, Hoffmann S, Engelhardt K, Zoidl G, and Dermietzel R (2011). Single cysteines in the extracellular and transmembrane regions modulate pannexin 1 channel function. The Journal of membrane biology 244, 21–33. [PubMed: 21938521]

Bunse S, Schmidt M, Prochnow N, Zoidl G, and Dermietzel R (2010). Intracellular cysteine 346 is essentially involved in regulating Panx1 channel activity. The Journal of biological chemistry 285, 38444–38452. [PubMed: 20829356]

Cahalan SM, Lukacs V, Ranade SS, Chien S, Bandell M, and Patapoutian A (2015). Piezo1 links mechanical forces to red blood cell volume. eLife 4.

Chao M-W, Chen C-P, Yang Y-H, Chuang Y-C, Chu T-Y, and Tseng C-Y (2016). N-acetylcysteine attenuates lipopolysaccharide-induced impairment in lamination of Ctip2-and Tbr1- expressing cortical neurons in the developing rat fetal brain. Scientific Reports 6, 32373. [PubMed: 27577752]

Chekeni FB, Elliott MR, Sandilos JK, Walk SF, Kinchen JM, Lazarowski ER, Armstrong AJ, Penuela S, Laird DW, Salvesen GS, et al. (2010). Pannexin 1 channels mediate 'find-me' signal release and membrane permeability during apoptosis. Nature 467, 863–867. [PubMed: 20944749]

Chiu YH, Schappe MS, Desai BN, and Bayliss DA (2018). Revisiting multimodal activation and channel properties of Pannexin 1. J Gen Physiol 150, 19–39. [PubMed: 29233884]

Choi DW (1987). Ionic dependence of glutamate neurotoxicity. The Journal of neuroscience : the official journal of the Society for Neuroscience 7, 369–379.

Cinar E, Zhou S, DeCourcey J, Wang Y, Waugh RE, and Wan J (2015). Piezo1 regulates mechanotransductive release of ATP from human RBCs. Proceedings of the National Academy of Sciences of the United States of America 112, 11783–11788. [PubMed: 26351678]

Cserép C, Pósfai B, Lénárt N, Fekete R, László ZI, Lele Z, Orsolits B, Molnár G, Heindl S, Schwarcz AD, et al. (2020). Microglia monitor and protect neuronal function through specialized somatic purinergic junctions. Science 367, 528–537. [PubMed: 31831638]

Davalos D, Grutzendler J, Yang G, Kim JV, Zuo Y, Jung S, Littman DR, Dustin ML, and Gan W-B (2005). ATP mediates rapid microglial response to local brain injury in vivo. Nature neuroscience 8, 752–758. [PubMed: 15895084]

Desplat A, Penalba V, Gros E, Parpaite T, Coste B, and Delmas P (2021). Piezo1-Pannexin1 complex couples force detection to ATP secretion in cholangiocytes. J Gen Physiol 153.

Diem K, Fauler M, Fois G, Hellmann A, Winokurow N, Schumacher S, Kranz C, and Frick M (2020). Mechanical stretch activates piezo1 in caveolae of alveolar type I cells to trigger ATP release and paracrine stimulation of surfactant secretion from alveolar type II cells. The FASEB Journal 34, 12785–12804. [PubMed: 32744386]

Dissing-Olesen L, LeDue JM, Rungta RL, Hefendehl JK, Choi HB, and MacVicar BA (2014). Activation of Neuronal NMDA Receptors Triggers Transient ATP-Mediated Microglial Process Outgrowth. The Journal of Neuroscience 34, 10511–10527. [PubMed: 25100586]

Dissing-Olesen L, and MacVicar BA (2015). Fixation and Immunolabeling of Brain Slices: SNAPSHOT Method. Current protocols in neuroscience / editorial board, Crawley Jacqueline N [et al] 71, 1 23 21–21 23 12.

Donkin JJ, and Vink R (2010). Mechanisms of cerebral edema in traumatic brain injury: therapeutic developments. Current opinion in neurology 23, 293–299. [PubMed: 20168229]

Dossi E, Blauwblomme T, Moulard J, Chever O, Vasile F, Guinard E, Le Bert M, Couillin I, Pallud J, Capelle L, et al. (2018). Pannexin-1 channels contribute to seizure generation in human epileptic brain tissue and in a mouse model of epilepsy. Science translational medicine 10.

Dreier JP, Lemale CL, Kola V, Friedman A, and Schoknecht K (2018). Spreading depolarization is not an epiphenomenon but the principal mechanism of the cytotoxic edema in various gray matter structures of the brain during stroke. Neuropharmacology 134, 189–207. [PubMed: 28941738]

Dzhala V, Valeeva G, Glykys J, Khazipov R, and Staley K (2012). Traumatic alterations in GABA signaling disrupt hippocampal network activity in the developing brain. The Journal of neuroscience : the official journal of the Society for Neuroscience 32, 4017–4031.

Eldadah BA, and Faden AI (2000). Caspase pathways, neuronal apoptosis, and CNS injury. J Neurotrauma 17, 811–829. [PubMed: 11063050]

Elmore Monica R.P., Najafi Allison R., Koike Maya A., Dagher Nabil N., Spangenberg Elizabeth E., Rice Rachel A., Kitazawa M, Matusow B, Nguyen H, West Brian L., et al. (2014). Colony-Stimulating Factor 1 Receptor Signaling Is Necessary for Microglia Viability, Unmasking a Microglia Progenitor Cell in the Adult Brain. Neuron 82, 380–397. [PubMed: 24742461]

Eyo UB, Gu N, De S, Dong H, Richardson JR, and Wu L-J (2015). Modulation of Microglial Process Convergence Toward Neuronal Dendrites by Extracellular Calcium. The Journal of Neuroscience 35, 2417–2422. [PubMed: 25673836]

Eyo UB, Peng J, Swiatkowski P, Mukherjee A, Bispo A, and Wu L-J (2014). Neuronal Hyperactivity Recruits Microglial Processes via Neuronal NMDA Receptors and Microglial P2Y12 Receptors after Status Epilepticus. The Journal of Neuroscience 34, 10528–10540. [PubMed: 25100587]

Eyo UB, and Wu LJ (2019). Microglia: Lifelong patrolling immune cells of the brain. Prog Neurobiol 179, 101614. [PubMed: 31075285]

Giannoni E, Buricchi F, Raugei G, Ramponi G, and Chiarugi P (2005). Intracellular reactive oxygen species activate Src tyrosine kinase during cell adhesion and anchorage-dependent cell growth. Molecular and cellular biology 25, 6391–6403. [PubMed: 16024778]

Giaume C, Saez JC, Song W, Leybaert L, and Naus CC (2019). Connexins and pannexins in Alzheimer's disease. Neuroscience letters 695, 100–105. [PubMed: 28893592]

Gottron FJ, Ying HS, and Choi DW (1997). Caspase inhibition selectively reduces the apoptotic component of oxygen-glucose deprivation-induced cortical neuronal cell death. Molecular and cellular neurosciences 9, 159–169. [PubMed: 9245499]

Hasbani MJ, Hyrc KL, Faddis BT, Romano C, and Goldberg MP (1998). Distinct roles for sodium, chloride, and calcium in excitotoxic dendritic injury and recovery. Exp Neurol 154, 241–258. [PubMed: 9875285]

Haynes SE, Hollopeter G, Yang G, Kurpius D, Dailey ME, Gan W-B, and Julius D (2006). The P2Y12 receptor regulates microglial activation by extracellular nucleotides. Nature neuroscience 9, 1512–1519. [PubMed: 17115040]

Heimer S, Knoll G, Schulze-Osthoff K, and Ehrenschwender M (2019). Raptinal bypasses BAX, BAK, and BOK for mitochondrial outer membrane permeabilization and intrinsic apoptosis. Cell death & disease 10, 556. [PubMed: 31324752]

Hines DJ, Hines RM, Mulligan SJ, and Macvicar BA (2009). Microglia processes block the spread of damage in the brain and require functional chloride channels. Glia 57, 1610–1618. [PubMed: 19382211]

Honda S, Sasaki Y, Ohsawa K, Imai Y, Nakamura Y, Inoue K, and Kohsaka S (2001). Extracellular ATP or ADP Induce Chemotaxis of Cultured Microglia through Gi/o-Coupled P2Y Receptors. The Journal of Neuroscience 21, 1975–1982. [PubMed: 11245682]

Hung SC, Choi CH, Said-Sadier N, Johnson L, Atanasova KR, Sellami H, Yilmaz O, and Ojcius DM (2013). P2X4 assembles with P2X7 and pannexin-1 in gingival epithelial cells and modulates ATP-induced reactive oxygen species production and inflammasome activation. PloS one 8, e70210. [PubMed: 23936165]

Ji J, Tyurina YY, Tang M, Feng W, Stolz DB, Clark RS, Meaney DF, Kochanek PM, Kagan VE, and Bayir H (2012). Mitochondrial injury after mechanical stretch of cortical neurons in vitro: biomarkers of apoptosis and selective peroxidation of anionic phospholipids. J Neurotrauma 29, 776–788. [PubMed: 21895519]

Karatas H, Erdener SE, Gursoy-Ozdemir Y, Lule S, Eren-Kocak E, Sen ZD, and Dalkara T (2013). Spreading depression triggers headache by activating neuronal Panx1 channels. Science 339, 1092–1095. [PubMed: 23449592]

Kato G, Inada H, Wake H, Akiyoshi R, Miyamoto A, Eto K, Ishikawa T, Moorhouse AJ, Strassman AM, and Nabekura J (2016). Microglial Contact Prevents Excess Depolarization and Rescues Neurons from Excitotoxicity. eNeuro 3.

Koval M, Schug WJ, and Isakson BE (2023). Pharmacology of pannexin channels. Current Opinion in Pharmacology 69, 102359. [PubMed: 36858833]

Lau AC, Cui H, and Tymianski M (2007). The use of propidium iodide to assess excitotoxic neuronal death in primary mixed cortical cultures. Methods in molecular biology 399, 15–29. [PubMed: 18309922]

Li Y, Du X. f., Liu C. s., Wen Z. l., and Du J. l. (2012). Reciprocal Regulation between Resting Microglial Dynamics and Neuronal Activity In Vivo. Developmental Cell 23, 1189–1202. [PubMed: 23201120]

Liang D, Bhatta S, Gerzanich V, and Simard JM (2007). Cytotoxic edema: mechanisms of pathological cell swelling. Neurosurg Focus 22, E2.

Lipton P (1999). Ischemic cell death in brain neurons. Physiol Rev 79, 1431–1568. [PubMed: 10508238]

Lohman AW, Billaud M, Straub AC, Johnstone SR, Best AK, Lee M, Barr K, Penuela S, Laird DW, and Isakson BE (2012a). Expression of Pannexin Isoforms in the Systemic Murine Arterial Network. Journal of Vascular Research 49, 405–416. [PubMed: 22739252]

Lohman AW, Weaver JL, Billaud M, Sandilos JK, Griffiths R, Straub AC, Penuela S, Leitinger N, Laird DW, Bayliss DA, et al. (2012b). S-nitrosylation inhibits pannexin 1 channel function. The Journal of biological chemistry 287, 39602–39612. [PubMed: 23033481]

Lohman AW, Weilinger NL, Santos SM, Bialecki J, Werner AC, Anderson CL, and Thompson RJ (2019). Regulation of pannexin channels in the central nervous system by Src family kinases. Neuroscience letters 695, 65–70. [PubMed: 28911820]

Mapps AA, Boehm E, Beier C, Keenan WT, Langel J, Liu M, Thomsen MB, Hattar S, Zhao H, Tampakakis E, et al. (2022). Satellite glia modulate sympathetic neuron survival, activity, and autonomic function. eLife 11, e74295. [PubMed: 35997251]

Merlini M, Rafalski VA, Ma K, Kim K-Y, Bushong EA, Rios Coronado PE, Yan Z, Mendiola AS, Sozmen EG, Ryu JK, et al. (2021). Microglial Gi-dependent dynamics regulate brain network hyperexcitability. Nature neuroscience 24, 19–23. [PubMed: 33318667]

Murana E, Pagani F, Basilico B, Sundukova M, Batti L, Di Angelantonio S, Cortese B, Grimaldi A, Francioso A, Heppenstall P, et al. (2017). ATP release during cell swelling activates a Ca2+-dependent Cl− current by autocrine mechanism in mouse hippocampal microglia. Scientific Reports 7, 4184. [PubMed: 28646166]

Okada Y, Okada T, Sato-Numata K, Islam MR, Ando-Akatsuka Y, Numata T, Kubo M, Shimizu T, Kurbannazarova RS, Marunaka Y, et al. (2019). Cell Volume-Activated and Volume-Correlated Anion Channels in Mammalian Cells: Their Biophysical, Molecular, and Pharmacological Properties. Pharmacol Rev 71, 49–88. [PubMed: 30573636]

Onami K, Kimura Y, Ito Y, Yamauchi T, Yamasaki K, and Aiba S (2014). Nonmetal haptens induce ATP release from keratinocytes through opening of pannexin hemichannels by reactive oxygen species. The Journal of investigative dermatology 134, 1951–1960. [PubMed: 24531690]

Palchaudhuri R, Lambrecht MJ, Botham RC, Partlow KC, van Ham TJ, Putt KS, Nguyen LT, Kim SH, Peterson RT, Fan TM, et al. (2015). A Small Molecule that Induces Intrinsic Pathway Apoptosis with Unparalleled Speed. Cell Rep 13, 2027–2036. [PubMed: 26655912]

Penuela S, Bhalla R, Nag K, and Laird DW (2009). Glycosylation regulates pannexin intermixing and cellular localization. Mol Biol Cell 20, 4313–4323. [PubMed: 19692571]

Penuela S, Kelly JJ, Churko JM, Barr KJ, Berger AC, and Laird DW (2014). Panx1 Regulates Cellular Properties of Keratinocytes and Dermal Fibroblasts in Skin Development and Wound Healing. Journal of Investigative Dermatology 134, 2026–2035. [PubMed: 24522432]

Prochnow N, Hoffmann S, Dermietzel R, and Zoidl G (2009). Replacement of a single cysteine in the fourth transmembrane region of zebrafish pannexin 1 alters hemichannel gating behavior. Experimental brain research 199, 255–264. [PubMed: 19701745]

Qu Y, Misaghi S, Newton K, Gilmour LL, Louie S, Cupp JE, Dubyak GR, Hackos D, and Dixit VM (2011). Pannexin-1 is required for ATP release during apoptosis but not for inflammasome activation. J Immunol 186, 6553–6561. [PubMed: 21508259]

Ranade SS, Qiu Z, Woo SH, Hur SS, Murthy SE, Cahalan SM, Xu J, Mathur J, Bandell M, Coste B, et al. (2014). Piezo1, a mechanically activated ion channel, is required for vascular development in mice. Proceedings of the National Academy of Sciences of the United States of America 111, 10347–10352. [PubMed: 24958852]

Reinehr R, Gorg B, Becker S, Qvartskhava N, Bidmon HJ, Selbach O, Haas HL, Schliess F, and Haussinger D (2007). Hypoosmotic swelling and ammonia increase oxidative stress by NADPH oxidase in cultured astrocytes and vital brain slices. Glia 55, 758–771. [PubMed: 17352382]

Rice ME (2000). Ascorbate regulation and its neuroprotective role in the brain. Trends in neurosciences 23, 209–216. [PubMed: 10782126]

Rieke K, Schwab S, Krieger D, von Kummer R, Aschoff A, Schuchardt V, and Hacke W (1995). Decompressive surgery in space-occupying hemispheric infarction: results of an open, prospective trial. Crit Care Med 23, 1576–1587. [PubMed: 7664561]

Rothman SM (1985). The neurotoxicity of excitatory amino acids is produced by passive chloride influx. The Journal of neuroscience : the official journal of the Society for Neuroscience 5, 1483–1489. [PubMed: 3925091]

Rungta RL, Choi HB, Tyson JR, Malik A, Dissing-Olesen L, Lin PJ, Cain SM, Cullis PR, Snutch TP, and MacVicar BA (2015). The cellular mechanisms of neuronal swelling underlying cytotoxic edema. Cell 161, 610–621. [PubMed: 25910210]

Sandilos JK, Chiu YH, Chekeni FB, Armstrong AJ, Walk SF, Ravichandran KS, and Bayliss DA (2012). Pannexin 1, an ATP release channel, is activated by caspase cleavage of its pore-associated C-terminal autoinhibitory region. The Journal of biological chemistry 287, 11303–11311. [PubMed: 22311983]

Sasaki Y, Hoshi M, Akazawa C, Nakamura Y, Tsuzuki H, Inoue K, and Kohsaka S (2003). Selective expression of Gi/o-coupled ATP receptor P2Y12 in microglia in rat brain. Glia 44, 242–250. [PubMed: 14603465]

Seminario-Vidal L, Okada SF, Sesma JI, Kreda SM, van Heusden CA, Zhu Y, Jones LC, O'Neal WK, Penuela S, Laird DW, et al. (2011). Rho signaling regulates pannexin 1-mediated ATP release from airway epithelia. The Journal of biological chemistry 286, 26277–26286. [PubMed: 21606493]

Shah PT, Yoon KW, Xu XM, and Broder LD (1997). Apoptosis mediates cell death following traumatic injury in rat hippocampal neurons. Neuroscience 79, 999–1004. [PubMed: 9219962]

Silverman W, Locovei S, and Dahl G (2008). Probenecid, a gout remedy, inhibits pannexin 1 channels. American Journal of Physiology-Cell Physiology 295, C761–C767. [PubMed: 18596212]

Simard JM, Kent TA, Chen M, Tarasov KV, and Gerzanich V (2007). Brain oedema in focal ischaemia: molecular pathophysiology and theoretical implications. Lancet Neurol 6, 258–268. [PubMed: 17303532]

Szalay G, Martinecz B, Lénárt N, Környei Z, Orsolits B, Judák L, Császár E, Fekete R, West BL, Katona G, et al. (2016). Microglia protect against brain injury and their selective elimination dysregulates neuronal network activity after stroke. Nature communications 7, 11499.

Thompson RJ, Jackson MF, Olah ME, Rungta RL, Hines DJ, Beazely MA, MacDonald JF, and MacVicar BA (2008). Activation of pannexin-1 hemichannels augments aberrant bursting in the hippocampus. Science 322, 1555–1559. [PubMed: 19056988]

Thompson RJ, Zhou N, and MacVicar BA (2006). Ischemia opens neuronal gap junction hemichannels. Science 312, 924–927. [PubMed: 16690868]

Torres JL, Palomino J, Moreno RD, and De los Reyes M (2017). Pannexin channels increase propidium iodide permeability in frozen–thawed dog spermatozoa. Reproduction, Fertility and Development 29, 2269–2276. [PubMed: 28390472]

Umpierre AD, and Wu L-J (2021). How microglia sense and regulate neuronal activity. Glia 69, 1637–1653. [PubMed: 33369790]

Vaarmann A, Gandhi S, and Abramov AY (2010). Dopamine induces Ca2+ signaling in astrocytes through reactive oxygen species generated by monoamine oxidase. The Journal of biological chemistry 285, 25018–25023. [PubMed: 20547771]

Wake H, Moorhouse AJ, Jinno S, Kohsaka S, and Nabekura J (2009). Resting Microglia Directly Monitor the Functional State of Synapses In Vivo and Determine the Fate of Ischemic Terminals. The Journal of Neuroscience 29, 3974–3980. [PubMed: 19339593]

Wang J, and Dahl G (2010). SCAM analysis of Panx1 suggests a peculiar pore structure. J Gen Physiol 136, 515–527. [PubMed: 20937692]

Weilinger NL, Lohman AW, Rakai BD, Ma EM, Bialecki J, Maslieieva V, Rilea T, Bandet MV, Ikuta NT, Scott L, et al. (2016). Metabotropic NMDA receptor signaling couples Src family kinases to pannexin-1 during excitotoxicity. Nature neuroscience.

Weilinger NL, Maslieieva V, Bialecki J, Sridharan SS, Tang PL, and Thompson RJ (2013). Ionotropic receptors and ion channels in ischemic neuronal death and dysfunction. Acta Pharmacol Sin 34, 39–48. [PubMed: 22864302]

Weilinger NL, Tang PL, and Thompson RJ (2012). Anoxia-induced NMDA receptor activation opens pannexin channels via Src family kinases. The Journal of neuroscience : the official journal of the Society for Neuroscience 32, 12579–12588. [PubMed: 22956847]

Weilinger NL, Wicki-Stordeur LE, Groten CJ, LeDue JM, Kahle KT, and MacVicar BA (2022). KCC2 drives chloride microdomain formation in dendritic blebbing. Cell Reports 41.

Wendt S, Johnson S, Weilinger NL, Groten C, Sorrentino S, Frew J, Yang L, Choi HB, Nygaard HB, and MacVicar BA (2022). Simultaneous imaging of redox states in dystrophic neurites and microglia at Aβ plaques indicate lysosome accumulation not microglia correlate with increased oxidative stress. Redox Biology 56, 102448. [PubMed: 36037587]

Whyte-Fagundes P, Kurtenbach S, Zoidl C, Shestopalov VI, Carlen PL, and Zoidl G (2018). A Potential Compensatory Role of Panx3 in the VNO of a Panx1 Knock Out Mouse Model. Frontiers in molecular neuroscience 11, 135. [PubMed: 29780304]

Wilde GJ, Sundstrom LE, and Iannotti F (1994). Propidium iodide in vivo: an early marker of neuronal damage in rat hippocampus. Neuroscience letters 180, 223–226. [PubMed: 7700583]

Xie H, Hou S, Jiang J, Sekutowicz M, Kelly J, and Bacskai BJ (2013). Rapid cell death is preceded by amyloid plaque-mediated oxidative stress. Proc Natl Acad Sci U S A 110, 7904–7909. [PubMed: 23610434]

Xu J, Chen L, and Li L (2018). Pannexin hemichannels: A novel promising therapy target for oxidative stress related diseases. Journal of cellular physiology 233, 2075–2090. [PubMed: 28295275]

Zhang J, Malik A, Choi HB, Ko RW, Dissing-Olesen L, and MacVicar BA (2014). Microglial CR3 activation triggers long-term synaptic depression in the hippocampus via NADPH oxidase. Neuron 82, 195–207. [PubMed: 24631344]

Zhang L, Deng T, Sun Y, Liu K, Yang Y, and Zheng X (2008). Role for nitric oxide in permeability of hippocampal neuronal hemichannels during oxygen glucose deprivation. J Neurosci Res 86, 2281–2291. [PubMed: 18381763]

Zhang X, Chen Y, Wang C, and Huang L-YM (2007). Neuronal somatic ATP release triggers neuron–satellite glial cell communication in dorsal root ganglia. Proceedings of the National Academy of Sciences 104, 9864–9869.

Zhou N, Gordon GR, Feighan D, and MacVicar BA (2010). Transient swelling, acidification, and mitochondrial depolarization occurs in neurons but not astrocytes during spreading depression. Cereb Cortex 20, 2614–2624. [PubMed: 20176688]

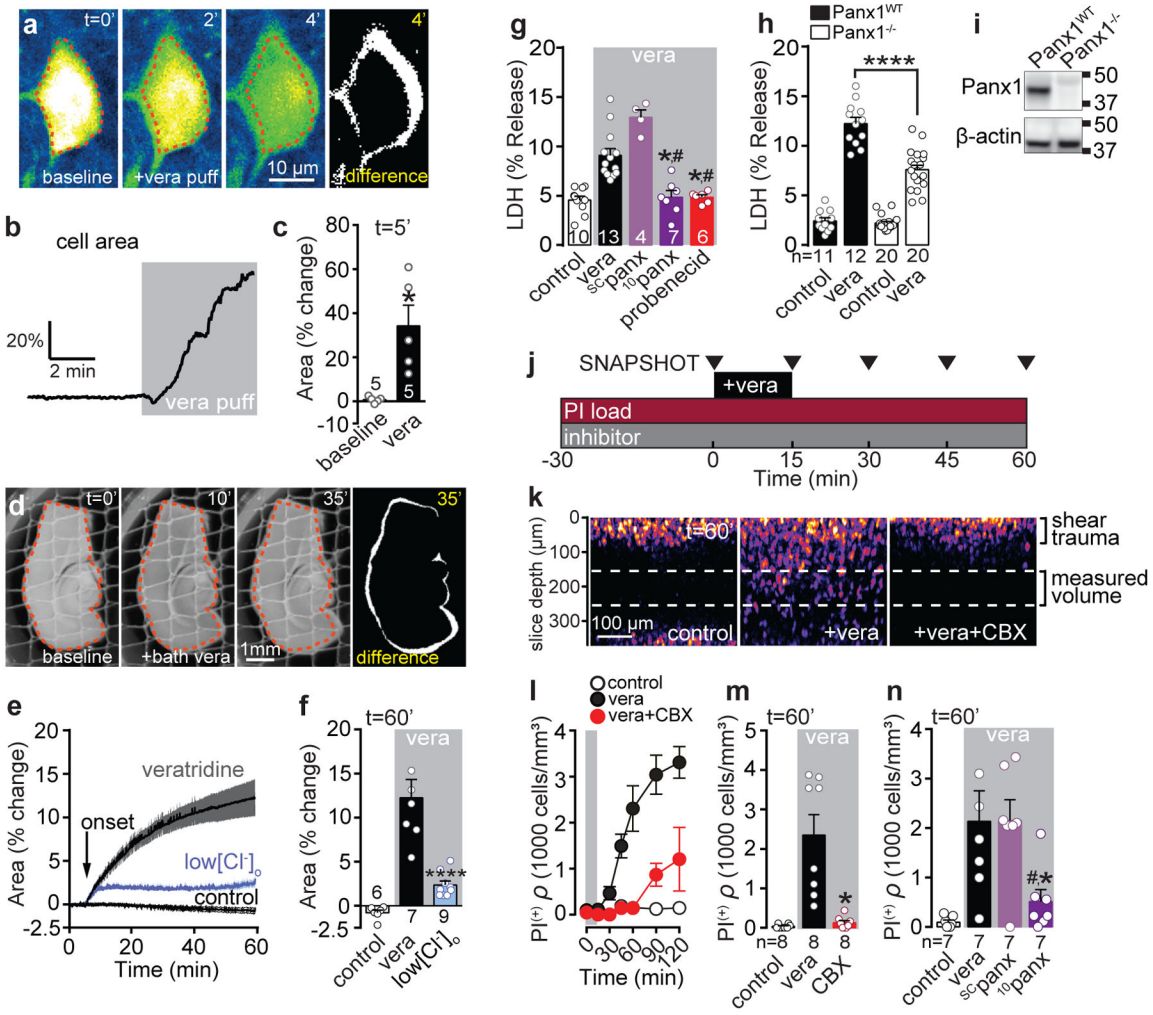

Figure. 1: Neuronal swelling leads to Panx1-dependent cell death.

a) Exemplar EGFP-expressing pyramidal neuron from rat exposed to veratridine (50 µM). Red dashed line denotes cell perimeter at baseline. **b**) Time course of veratridine induced swelling measured as cross-sectional area. **c**) Average change in area after 5 min exposure to veratridine (paired t-test, *P<0.05). **d**) Whole-tissue swelling imaged at low magnification during bath application of veratridine. Red dashed line denotes slice perimeter at baseline. **e&f**) Average veratridine-evoked changes in slice area are reduced in low$[Cl^-]_o$ (Tukey Test, *P<0.05). **g)** Quantitative summary of veratridine-induced LDH release at 90 min. Pretreating tissue with pannexin inhibitors ^{10}panx (100 µM) or probenecid (1 mM) attenuated LDH release compared to veratridine or ^{SC}panx (100 µM) (Tukey Test, *P<0.05 vs vera, $^{\#}$P<0.05 vs vera+^{SC}panx). **h**) LDH release is reduced in Panx$^{-/-}$ mice compared to Panx1^{WT} (Tukey Test, ****P<0.0001). **i**) Panx1 expression is not detectable by western blot in tissue collected from Panx1$^{-/-}$ mice. **j)** Experimental paradigm for imaging swelling-dependent PI-loading using the 'SNAPSHOT' flash-fixation method (Dissing-Olesen and MacVicar, 2015). **k**) Orthogonal XZ maximum intensity projection image of rat L4/5 cortical neurons from a 3D XYZ stack series at 60' post veratridine. PI loading was blocked with CBX (100 µM). **l**) Time course of PI uptake (15 min veratridine application indicated

by gray box). **m&n)** PI^+ cell count is reduced in CBX and ^{10}panx treated tissue (Tukey Test, *P<0.05 vs veratridine alone, $^{\#}$P<0.05 vs veratridine +^{SC}panx).

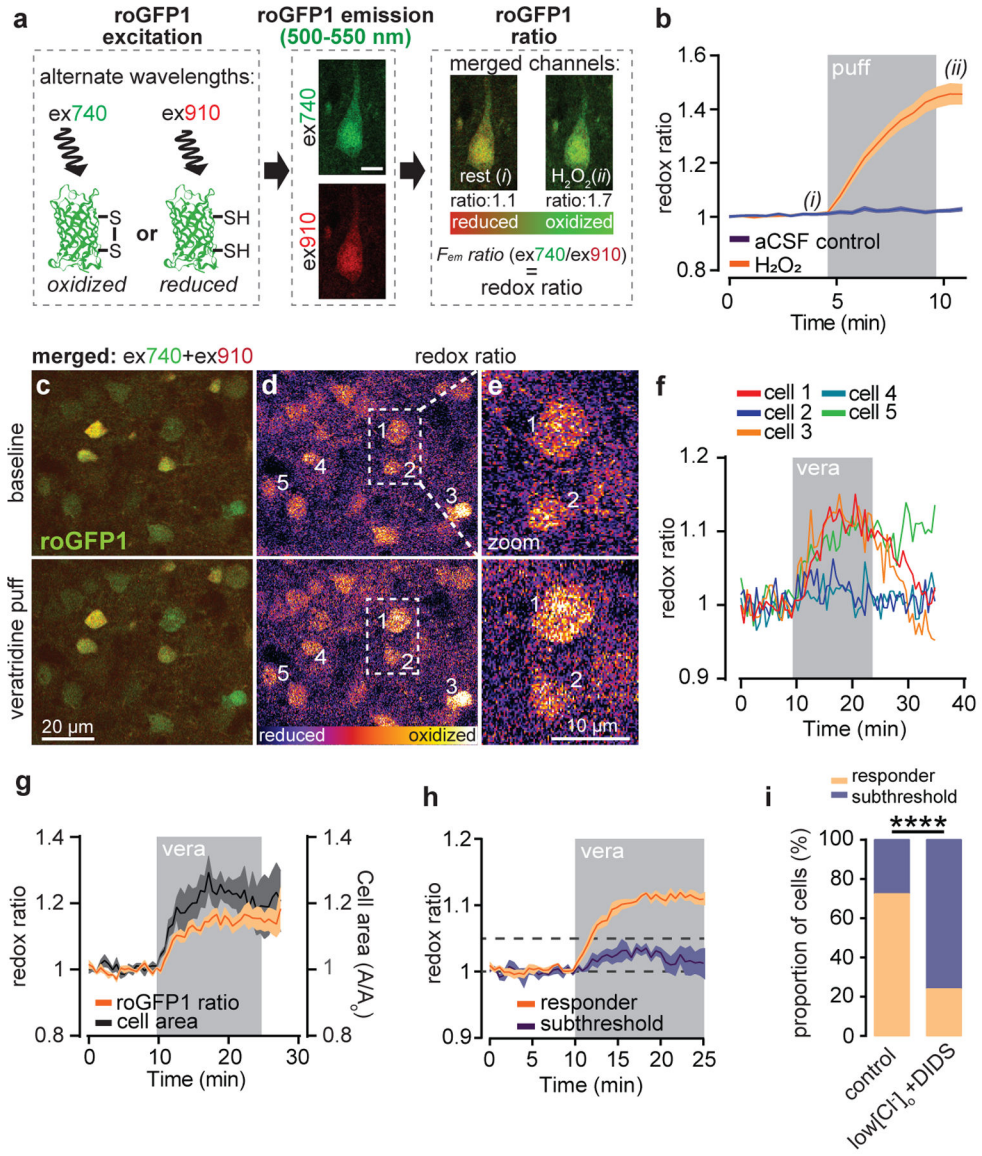

Figure 2: Neuronal swelling triggers oxidative stress.

a) Imaging pipeline of the ratiometric redox sensor roGFP1. Measuring the ratio of emission between Excitation at 740 nm or 910 nm will report the cytosolic redox state (pseudocolour-coded green and red for oxidation and reduction, respectively). **b)** Validation of roGFP1 sensitivity to H_2O_2 (8 mM) in virally transfected rat neurons. Trace labels '*i*' and '*ii*' correspond to 'rest' and 'H_2O_2' example mean images from 'a'. **c)** Representative merged images (740 and 910 nm excitation channels) of roGFP1-expressing cortical neurons before and after local veratridine puff. **d)** Pseudocoloured images of the oxidized/reduced emission ratio. **e)** Zoomed images from boxes in 'd'. **f)** Changes to roGFP1 ratios from representative cells in 'c'. **g)** Average change in neuronal roGFP1 ratio and cell area over time in veratridine. Data are presented as mean ± sem. **h)** Average change in ex740/ex910 ratio during 15' veratridine puff reveal a bimodal population of responding (i.e. oxidizing) cells. **i)** Proportion of imaged cells that oxidized in veratridine alone (control, n=58 cells, 9

experiments from 6 animals) and veratridine in low Cl^-/DIDS to block swelling (n=46 cells, 7 experiments from 6 animals, Fisher's exact test ****P<0.0001).

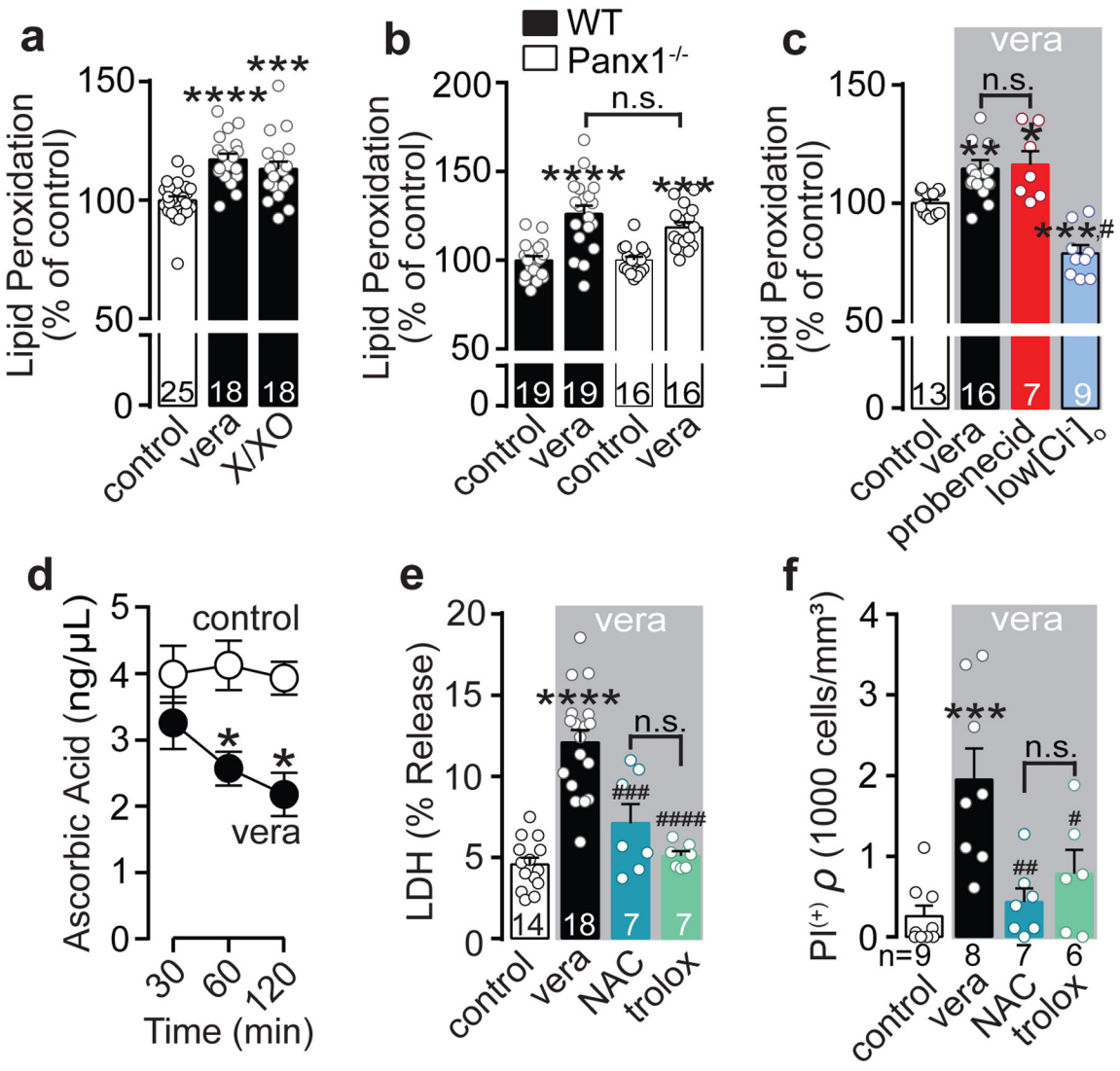

Figure 3: Buffering oxidative stress is neuroprotective during swelling.

a) Quantitative comparison between veratridine- (****P<0.0001) and X/XO-induced lipid peroxidation (***P= 0.0006 from rat brain tissue compared to control, Tukey Test). **b&c**) Lipid peroxidation levels were not reduced in Panx1$^{-/-}$ mice compared to Panx1^{WT} mice (****P<0.0001 and ***P=0.0005 compared to controls, respectively), nor in slices treated with probenecid, but was decreased in low$[Cl^-]_o$, Tukey Test, ***P=0.0009 vs control, $^{\#}$P<0.0001 vs veratridine. **d**) Prolonged exposure to veratridine decreases ascorbic acid concentration from acute slice lysate over time, Tukey Test, *P<0.05 compared to control condition. **e**) Veratridine-induced LDH release (****P<0.0001 vs control) was significantly reduced in the presence of ROS buffers NAC (5 mM, $^{\#\#\#}$P=0.0004 vs vera) and Trolox (100 µM, $^{\#\#\#\#}$P<0.0001 vs vera), Tukey Test. **f**) PI-uptake in veratridine. Data are presented as mean± sem.

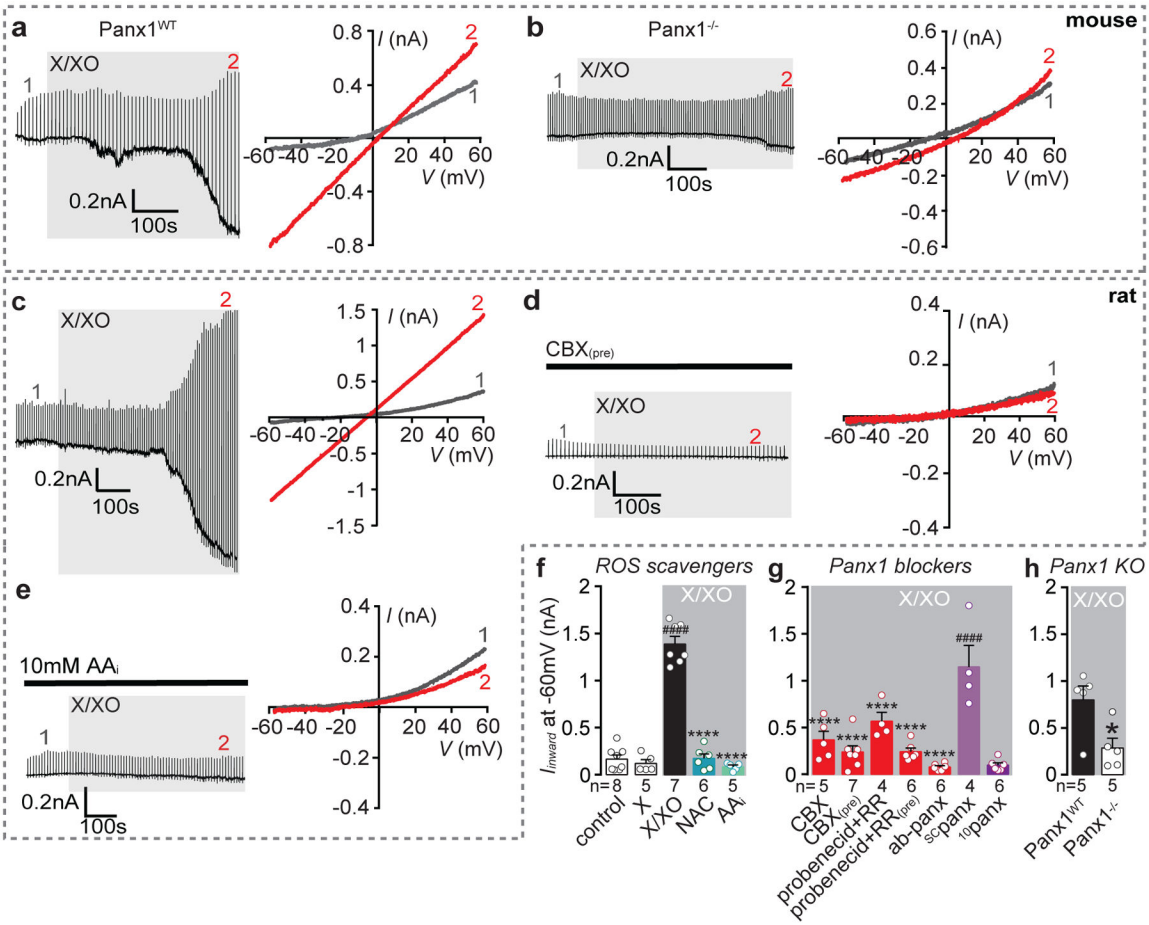

Figure 4: ROS directly activates Panx1 channels.

a&b) Whole-cell electrophysiology recordings from pyramidal neuron acutely isolated from Panx1^{WT} and Panx1$^{-/-}$ murine tissue. Left panels: bath application of X/XO activated Panx1 currents in Panx1^{WT} but not in Panx1$^{-/-}$ cells. Right panels: example voltage ramps show a typical linear Panx1 current (trace '2') that is absent in Panx1$^{-/-}$. **c&d**) Exemplar recordings from rat pyramidal neurons revealed a X/XO- induced current that was blocked by pre-application of CBX. **e)** Buffering ROS with intracellular application of AA (AA_i 10 mM) prevented Panx1 opening. **f&g**) Quantification of X/XO-driven inward currents. Current amplitudes in rat were significantly reduced by ROS scavengers NAC and AA (Tukey Test, *P<0.05 to 'X/XO', $^{\#}$P<0.05 to 'control' and 'X'), by Panx1 inhibitors CBX, probenecid, the c-terminal Panx1 antibody (ab-Panx1) (Tukey Test, *P<0.05 to 'X/XO', $^{\#}$P<0.05 to 'control' and 'X'), and ^{10}panx (Tukey Test, *P<0.05 to '^{SC}panx') compared to X/XO alone. **h**) X/XO-Panx1 currents in mice were significantly reduced in Panx$^{-/-}$ vs Panx1^{WT} (two-tailed t-test, *P<0.05). Data are presented as mean ± sem.

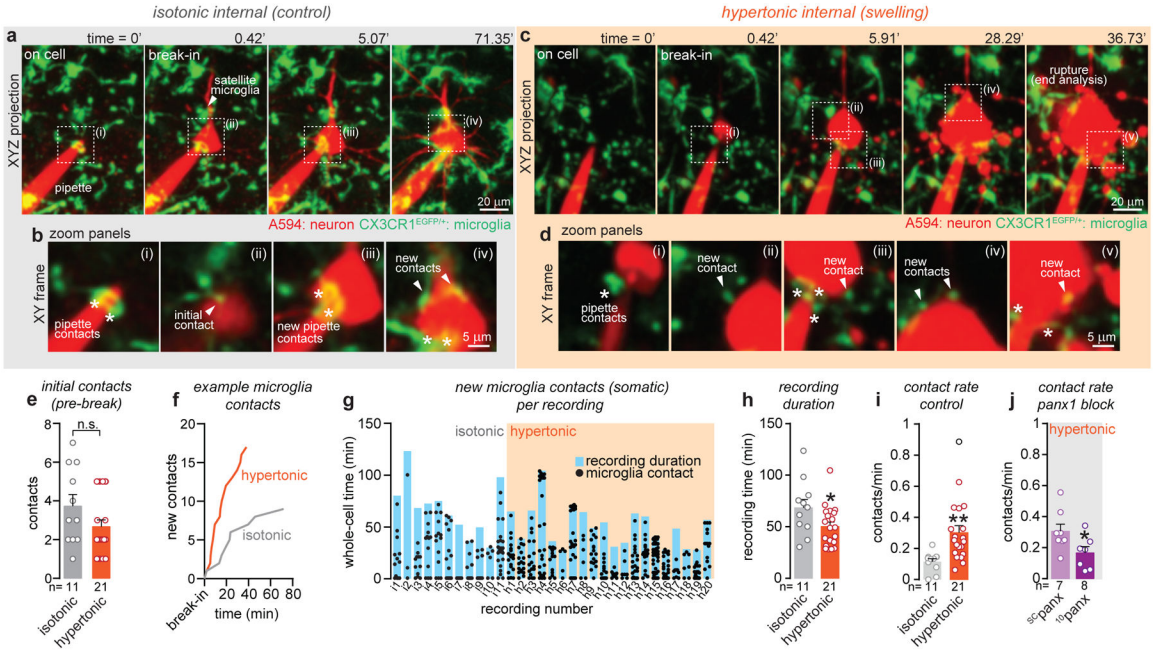

Figure 5: Panx1 opening recruits microglia-neuron contacts.

a-d) Example imaging sequence of L4 neuron from a CX3CR1$^{EGFP/+}$ mouse dialyzed with an isotonic recording solution containing Alexa-594 via whole-cell patch clamp. **a)** maximum intensity projections (i.e. collapsed XYZ stack) showing overview of microglia contacts on the neuronal soma pre- and post-break-in to whole-cell mode. Note satellite microglia could be identified post-break-in. **b)** zoomed single XY plane images of regions of interest corresponding to white boxes with roman numerals in the XYZ projections. Pipette contacts (asterisks) were separately categorized from initial and new contacts (arrows). **c&d)** Image time series of exemplar L4 neuron patch-loaded with a hypertonic recording solution to induce osmotic swelling shows increased microglia contacts. Membrane rupture and dye loss at t= 36.73 min. **e)** Initial contacts counted from the first image post-break. **f)** Example time courses of microglia-somatic contacts in an isotonic (control) and hypertonic experiment. **g)** Summary data illustrating the timestamps for microglia contacts over the duration of each recording. **h)** Quantification of recording times for isotonic and hypertonic experiments. **i)** Microglia contact rate is increased in hypertonic conditions (**P=0.0052 two-tailed t-test). **j)** Microglia contact rate is significantly reduced with bath applied 10panx compared to the scrambled control peptide (*P=0.0426, two-tailed t-test).

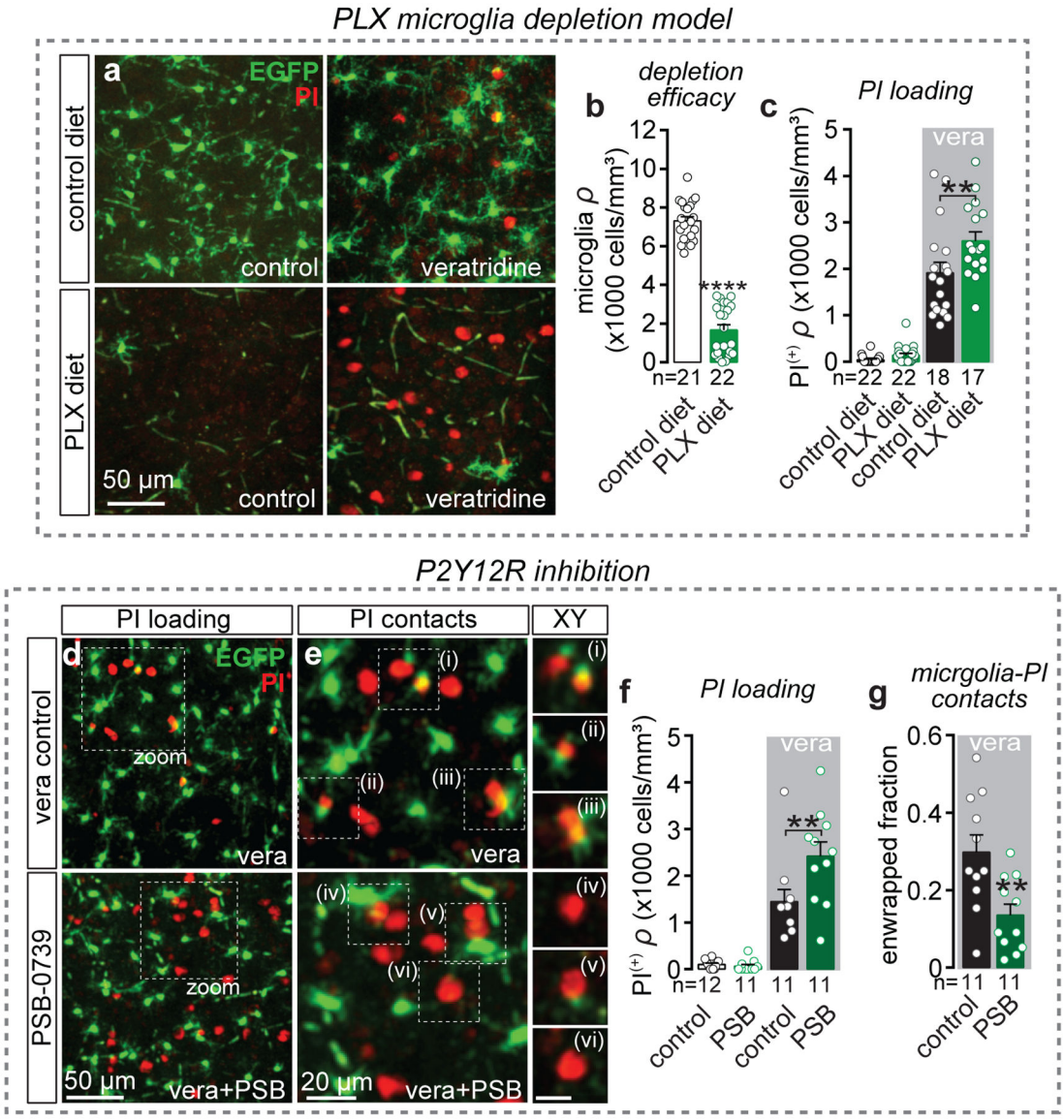

Figure 6: Microglia-neuron contacts are neuroprotective in cytotoxic edema.

a) Representative XYZ projection images (100 µm volume depth) of PI loaded neurons from CX3CR1$^{EGFP/+}$ mice on control (top row) or PLX (bottom row) diets with and without veratridine. **b)** Quantification of microglia density in cortex from mice on control vs PLX diet (****P<0.0001, two-tailed t-test). **c)** PI loading quantification of control vs PLX diets with and without veratridine (**P=0.0043, one-way ANOVA, Tukey test). **d)** Example XYZ maximum intensity projection images PI loading in veratridine alone and in combination with PSB. **e)** Exemplar XYZ maximum intensity projection images of PI-positive neurons enwrapped by microglia processes in control (vera only, top panels) and vera+PSB conditions (bottom panels). (right panels) single zoom XY-plane examples of PI-positive neurons and associated microglia processes (scale = 10 µm). **f)** PI quantification showing increased cell death when veratridine is applied in the presence of PSB (**P= 0.0065, one-way ANOVA, Tukey test). **g)** Quantification of the fraction of PI-positive cells

enwrapped by microglia processes showing a reduction in microglia-neuron associations in PSB (**P= 0.0062, two-tailed t-test).

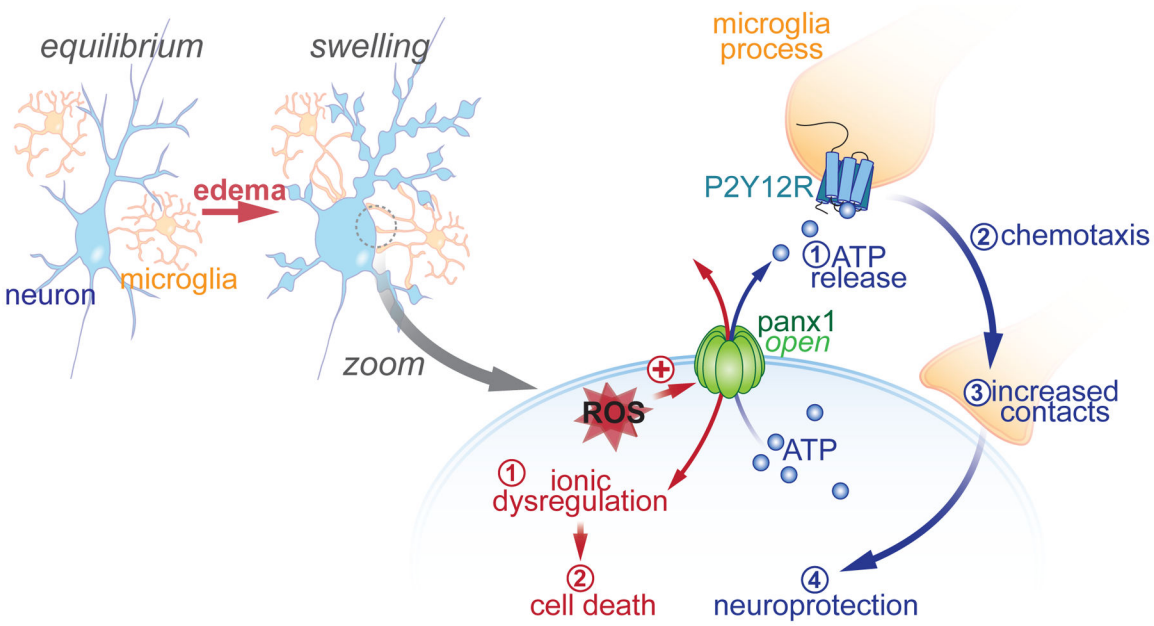

Figure 7: Summary of findings.

Neuronal swelling in edema triggers an increase in cytosolic ROS, leading to downstream Panx1 channel opening with dichotomous consequences. On one hand, Panx1 opening causes ionic dysregulation leading to cell death. On the other hand, ATP release through Panx1 attracts processes from neighbouring microglia, which contact swelling neurons to exert a neuroprotective effect.